

Rivers occupy self-formed channels. A channel is a topographic feature with identifiable banks created by running water. Our discussions in this chapter focus on channels formed by rivers in sediments deposited by the river. These are called alluvial channels. (Alluvium is sediment deposited by flowing streams, a word derived from the Latin – of course – *alluvius*, which means “washed against.” Hence, alluvial is an adjective meaning of, related to, or derived from alluvium.) There are also bedrock channels, in which the channel is cut into solid rock, rather than loose sediment (see Chapter 13). River channels are self-formed in that they construct their channel form, their longitudinal profile, the height of the banks and the width of the floodplain. We have already described how the river network displays geometrical self-similarity, and how this feature is in common among systems designed to convey some spatially distributed property – here water. River discharge commonly increases monotonically downstream. But we must ask just how the channel adjusts in order to carry this increasing discharge – does it adjust its width, its depth, its speed? This falls under the realm of the hydraulic geometry of a channel. We also acknowledge that the river’s discharge will vary in time, as it is made to carry water from precipitation and snowmelt that vary on seasonal and synoptic weather timescales. What hydraulic properties does the river change in order to accommodate the variations in discharge at a point? These timescales are too short for the entire channel geometry to change. The flow increases in stage (water depth) as discharge increases, until some point at which the water can no longer be conveyed within the channel. It then spills out of the banks, it floods, and spreads across the floodplain adjacent to the channel. The flood plain is therefore a part of the river.

We also describe the dominant plan view shapes of river channels – meandering and braided forms. We must rely upon knowledge both of the three-dimensional structure of the water flowfield, and of the mechanics of sediment transport that we discuss in detail in Chapter 14.

Another important element of the river is its longitudinal profile. In contrast to hillslopes, which generally increase in slope with distance from the divide, rivers decline in slope with distance down-valley, giving rise to the concave up profile. We discuss why rivers behave so differently, and what governs their

profiles. This includes a discussion of baselevel, the elevation to which the river grades in the long term.

We close with a description of recent work on the largest river system in the world, the Amazon, using it as an example of how one can employ both first-order treatments that again go back to the principles of conservation, and marry these with modern methods of field investigation.

Theory and measurement of turbulent flows in open channels

The flow of water when it is confined within a channel belongs to a class of fluid mechanics problem termed open channel hydraulics. We first discuss the theory of open channel flow, from which we derive equations for surface and mean velocity profiles, and for discharge. This sets us up to discuss the means by which discharge is measured.

In this section we will develop one of the more famous equations in fluid mechanics, the law of the wall, which describes the theory of flow near boundaries. In our case, the most important “wall” or boundary of the flow is in fact its base, the channel bed. The law of the wall will lead the way toward understanding the “six-tenths” rule, a rule of thumb for the depth at which the flow velocity equals the mean velocity. We can then compare the formal approach with more empirically based approaches that have long been used in assessing mean flow velocities and discharge within open channels, including the Manning’s, Chezy, and Darcy–Weisbach equations. Finally, we summarize methods used to measure discharge in a channel, including those based upon space-borne instruments.

In almost all geomorphically relevant situations, the flow of water over the land surface is turbulent. Experimentally, when the channel Reynolds number exceeds a critical value of about 2000, the flow in an open channel is turbulent. Recall that the Reynolds number is the ratio of inertial to viscous forces, defined for a channel as $Re = H\langle u \rangle / \nu$, where H is the channel depth, $\langle u \rangle$ is the mean velocity, and ν is the kinematic viscosity. At high Re , inertia reigns over viscosity; momentum and all other scalar quantities are moved about within the flow by exchange of macroscopic packets of fluid, rather than by molecular collisions. We must therefore develop an equation that captures the physics of turbulent flows.

As always, our strategy for developing the velocity structure within a flow will be to start with the profile of shear stress, relate the stress to the strain rate through appeal to some rheological relationship, and then

integrate the strain rate profile to yield the velocity profile, $U(z)$, where U is the velocity in the downstream (x) direction, and z is taken to be vertically upward from the bed.

Box 12.1 Steady, uniform, open channel flow assumptions

We will use the x -component of the Navier–Stokes equation (see Equation 12.69, developed in the appendix to this chapter) and solve it for the particular flow situation. We often begin by assuming that open channel flows are steady and uniform. More formally, here are the assumptions and the resulting simplifications to the Navier–Stokes equation:

- *The flow is steady.* This allows us to set all derivatives with respect to (w.r.t.) time to zero. The first term on the left-hand side of Equation 12.69 vanishes.
- *The flow is horizontally uniform.* This allows us to ignore terms with gradients in x and y . The second and third terms on the left-hand side of Equation 12.69 vanish, and the second derivatives w.r.t. x and y vanish on the right-hand side.
- *The flow is entirely driven by the downslope component of gravity, $g_x = g \sin(\theta)$.* The pressure gradient is assumed to be negligible, as the flow thickness is uniform in the channel. The second term on the right-hand side of Equation 12.69 vanishes.
- *There is no flow through the bottom of the channel, in either direction.* This requires that the vertical velocity of the flow, $w = 0$ at $z = 0$. From continuity in an incompressible medium, we know that $\partial u/\partial x + \partial v/\partial y + \partial w/\partial z = 0$. Horizontally uniform conditions require that the first two terms vanish, leaving $\partial w/\partial z = 0$. Integrating this yields $w = \text{constant}$. The boundary condition of no flow through the boundary allows us to assess this constant to be zero. Since $w = 0$ everywhere on the bed ($z = 0$), the last term on the right-hand side of Equation 12.69 = 0, meaning that the entire left-hand side of the equation = 0. (Note, having dispensed with v and w , we will use U , rather than u , for velocity in the x direction for the rest of the chapter, as U is easier to distinguish from the u^* and v parameters we will encounter shortly.)

Given these assumptions, the x -component of the Navier–Stokes equation then becomes

$$0 = g_x + \nu \frac{\partial^2 u}{\partial z^2} \quad (12.1)$$

For laminar flow in which $Re \ll 1$, the viscosity can be taken to be uniform, and we may simply integrate the equation to obtain the gradient of the velocity:

$$\frac{\partial u}{\partial z} = -\frac{\rho_f g \sin(\theta)}{\mu} z + c_1 \quad (12.2)$$

where c_1 is a constant of integration, and the kinematic viscosity, ν , is shown as the ratio of the dynamic viscosity and fluid density, μ/ρ_f . In open channel flow, we may safely assume that the velocity gradient vanishes at the top of the flow, as there is no overlying fluid exerting a shear stress on the fluid in the channel. Therefore, at $z = H$, $\partial u/\partial z = 0$ and

$$c_1 = \frac{\rho_f g \sin(\theta)}{\mu} H$$

so that Equation 12.2 becomes:

$$\frac{\partial U}{\partial z} = \frac{\rho_f g \sin(\theta)}{\mu} (H - z) \quad (12.3)$$

Box 12.1 (cont.)

Integrating once more yields

(12.4)

$$u = \frac{\rho_f g \sin(\theta)}{\mu} \left(Hz - \frac{z^2}{2} \right) + c_2$$

where c_2 is our second constant of integration. This we evaluate knowing that the flow speed goes to zero at the boundary (the no-slip boundary condition), in which case c_2 vanishes and we have for our final flow velocity profile:

(12.5)

$$u = \frac{\rho_f g \sin(\theta)}{\mu} \left(Hz - \frac{z^2}{2} \right)$$

This is the solution for a low Re, laminar flow velocity profile.

In simple flows, in particular those that are steady and uniform, the shear stress increases linearly with depth into the fluid, at a rate dictated by the density of the fluid:

$$\tau_{zx} = \rho_f g \sin(\theta)(H - z) \quad (12.6)$$

The next few steps show how one can derive this equation directly from application of Cauchy's law (developed in the appendix to this chapter). If the flow is steady, incompressible and uniform, we may neglect the left-hand side of Equation 12.63, and the second derivatives with respect to x and y on the right-hand side. The pressure gradient may be neglected relative to the gravitational force. This leaves simply

$$0 = \rho_f g_x + \frac{\partial \tau_{zx}}{\partial z} \quad (12.7)$$

which we can integrate once to obtain the stress profile:

$$\tau_{zx} = -\rho_f g_x z + c \quad (12.8)$$

The constant of integration, c , can be evaluated by appeal to the fact that at the top of the flow, at $z = H$, the shear stress vanishes. This means that

$$c = \rho_f g_x H \quad (12.9)$$

and

$$\tau_{zx} = \rho_f g_x (H - z) = \rho_f g \sin(\theta)(H - z) \quad (12.10)$$

as in Equation 12.6. Equations 12.6 or 12.10 show that the shear stress increases linearly from the surface (at $z = H$) to the bed (at $z = 0$) of the flow.

The stress reaches a maximum at the bed of

$$\tau_b = \rho_f g H \sin(\theta) \quad (12.11)$$

The subscript "b" in τ_b can be thought of as meaning bed, basal, or boundary.

It is the rheology, or, in the case of a fluid, the relationship between the strain rate and the stress, that makes this problem difficult. In the case of laminar flow (low Reynolds number, the strain is proportional to the shear stress, as first outlined in Chapter 8 (see Figure 8.10)). The proportionality constant is the inverse of the fluid viscosity, a temperature-dependent parameter you can look up in reference books. The strain rate of the fluid (equivalent to the vertical velocity profile) is then simply the product of the inverse of viscosity with the stress:

$$\dot{\epsilon} = \frac{dU}{dz} = \frac{1}{\mu} \tau_{zx}$$

$$\frac{dU}{dz} = \frac{1}{\mu} \rho_f g (H - z) \sin(\theta) \quad (12.12)$$

In the case of turbulent flows, however, the rheology is intimately controlled by the flow itself, rather than by the material properties of the substance that is flowing. That is, the efficiency with which momentum is transported from place to place in the flow depends upon the flow structure, the vigor of the flow, and the size of the eddies doing the mixing. In a turbulent flow, the momentum is being moved about by macroscopic whorls within the flow, blobs of fluid trading places with each other, their momenta intact. The relative efficiency of momentum exchange under this mechanism vs. that associated with molecular collisions (the root of viscosity), is expressed by the Reynolds number, Re:

$$\text{Re} = \frac{\rho_f UH}{\mu} = \frac{UH}{\nu} \quad (12.13)$$

The second expression takes advantage of the definition of the kinematic viscosity of a fluid, $\nu = \mu/\rho$. The Reynolds number is another of those famous non-dimensional numbers we run across in fluid mechanics and geomorphology (others being the Mach number, Froude number, and Rouse number). They are named for famous mechanicians, in this case, Sir Osborne Reynolds (1843–1912), who experimented with turbulent flows in the mid-nineteenth century. In this instance the relevant length scale is the thickness of the flow, H , and the velocity is the mean vertically averaged velocity $\langle U \rangle$; this version of the Reynolds number is called the channel Reynolds number. (See our discussion of settling velocity in Chapter 10 for another application, in which we had to define a grain or particle Reynolds number.) Take for example a relatively benign river of depth 1 m, mean velocity 1 m/s. As the kinematic viscosity of water is $0.01 \text{ cm}^2/\text{s}$, or $1 \times 10^{-6} \text{ m}^2/\text{s}$, the Reynolds number of this typical river flow is then 10^6 . This is roughly three orders of magnitude above the empirically determined threshold for turbulence in an open channel (of 500–2000), meaning that we are quite safe in assuming that the flow will be turbulent.

It is clear from inspection of the measured instantaneous profiles in a flow that we haven't a prayer of writing an equation for the instantaneous flow field. Each profile varies significantly from the others, reflecting the passage of eddies past the instrument site. Calculation of two- and three-dimensional turbulent structures is a challenge even for the modern fluid mechanician, requires heavy computation, and even so depends entirely upon a choice of initial velocity structure. Instead, we will seek a theory for the *temporally* averaged flow velocity at a point in the flow. (Note the emphasis on temporal; we seek a spatial average of this temporally averaged flow later.) Symbolically, we may decompose the flow into a mean quantity and a time-varying quality, $U = \bar{U} + u'$, where the bar denotes the *time averaging* (note the distinction from $\langle U \rangle$, which is the depth-averaged velocity). We seek an expression for the profile of mean velocity with height above the bed: $\bar{U}(z)$. This decomposition of the velocity is what Reynolds accomplished in his 1895 paper (Reynolds, 1895).

We wish to know how efficient the flow is at transporting momentum, and what the spatial structure of this efficiency is. Said another way, we wish to know

the "effective viscosity" of the flow. By analogy with the viscous (low Re) case, this efficiency has been named the eddy viscosity, and the rheological equation (relating strain rate, dU/dz , to shear stress, τ) is cast as

$$\tau = \rho_f K \frac{d\bar{U}}{dz} \quad (12.14)$$

where K is the eddy viscosity, and has dimensions of L^2/T . It has been shown through experimental measurement of the strain rate as a function of the distance from a boundary, that relatively close to a boundary the eddy viscosity increases linearly with the distance from the boundary, or, in our case, with the height above the bed of the channel:

$$K = k u_* z \quad (12.15)$$

where z is the height above the bed, u_* is a characteristic velocity called the shear velocity $= \sqrt{\tau_b/\rho_f}$, and k is a non-dimensional scalar, named von Karman's constant after a famous German aeronautical engineer. This is plotted in Figure 12.1. Experiments show that $k = 0.40$. Note that this eddy viscosity is nowhere near uniform within the flow, close to the boundary. The most efficient part of the flow will be far from the boundary, reflecting the fact that here larger eddies can very efficiently exchange momentum.

We can now combine the expression for shear stress structure with the rheological rule in Equation 12.14 to derive the expected strain rate profile. There is one trick. We make use of the fact that the portion of the flow we are most interested in is very close to the bed. We approximate the shear stresses (τ) as being uniform within this region, equal to the basal shear stress, τ_b . This is shown graphically with a vertical line segment in Figure 12.1(a). The characteristic velocity we defined above, $u_* = \sqrt{\tau_b/\rho_f}$, can be rearranged to find $\tau_b = \rho_f u_*^2$. Given these assumptions, the shear strain rate becomes

$$\frac{d\bar{U}}{dz} = \frac{u_*}{kz} \quad (12.16)$$

The strain rate should diminish with height above the bed, not linearly as in the viscous case shown in Equation 12.12, but more rapidly – hyperbolically in the turbulent case. Not only is the stress diminishing with height into the flow, but the efficiency of the flow in exchanging momentum is increasing.

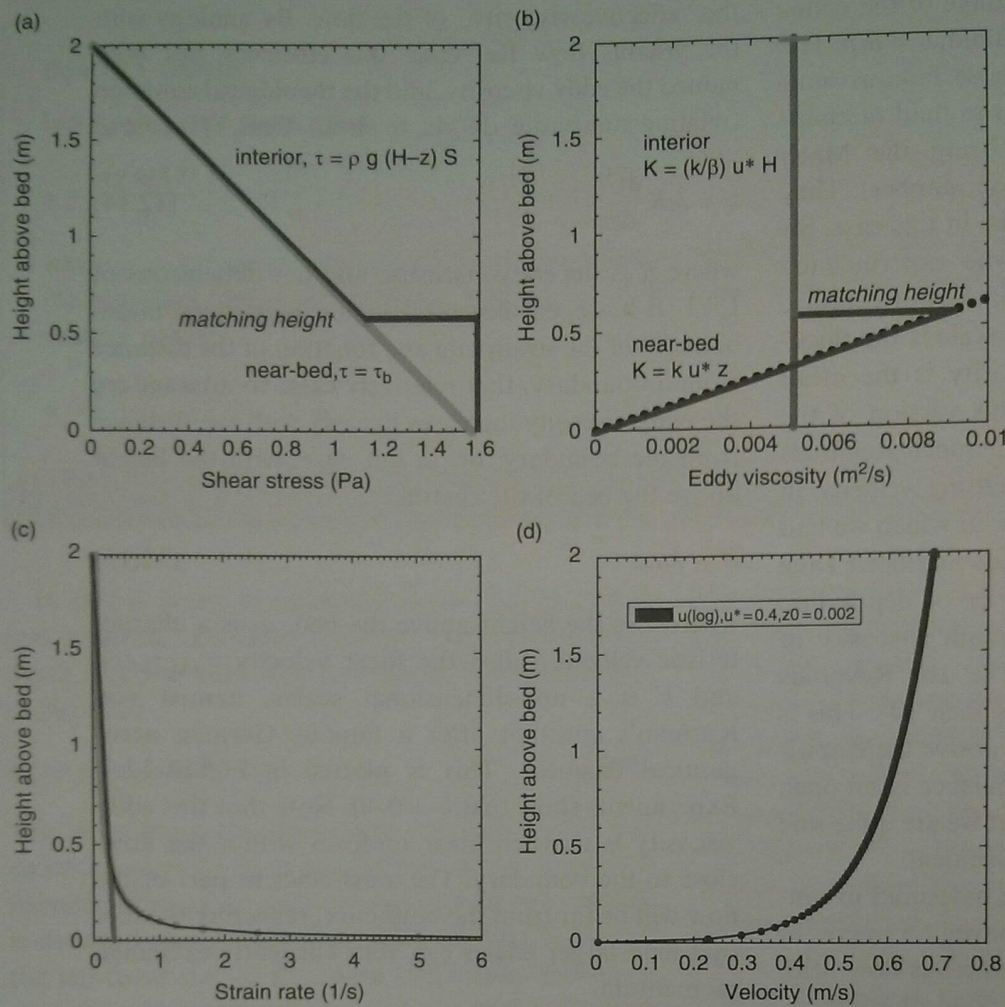


Figure 12.1 Distribution of (a) shear stress, (b) eddy viscosity, (c) strain rate, and (d) velocity in a turbulent flow of 2 m depth. The flow is broken into two regions: a near-bed boundary layer in which the shear stress is assumed to be approximately constant, and an interior region in which the shear stress declines to zero at the top. The corresponding eddy viscosity structure shown in (b) shows linearly increasing eddy viscosity with height above the bed in the boundary layer, and uniform eddy viscosity in the interior. The strain rate profile must be continuous, which determines a matching height where the strain rate from the boundary layer (black line in (c)) equals the strain rate from the interior flow (grey line in (c)). This strain rate profile is integrated to yield the expected velocity profile shown in (d).

In order to calculate the velocity profile, we must integrate this equation, yielding

$$\bar{U} = \frac{u_*}{k} \ln(z) + c \tag{12.17}$$

where c is a constant of integration. We assess the constant of integration by appeal to a known or measurable value of the variable we are integrating, here the velocity, at some particular position within the flow. In turbulent flows, this is traditionally done by assigning the flow velocity to go to zero at a specific (but fictional) height above the bed, known as z_0 . This is known as “z-nought,” or “Nikuradse’s roughness” (about which more later). The constant then becomes

$$c = -\frac{u_*}{k} \ln(z_0) \tag{12.18}$$

and the final equation for the time-averaged flow velocity profile becomes

$$\bar{U} = \frac{u_*}{k} \ln\left(\frac{z}{z_0}\right) \tag{12.19}$$

This is the famous “law of the wall,” which holds true in the region of a turbulent flow that is quite close to a boundary, or wall. It is shown in Figure 12.2. The flow increases logarithmically with distance into the fluid, the greatest strain rate (or, equivalently, gradient in the mean velocity) being closest to the wall. We show an example of flow data from the Mississippi River in Figure 12.3, in which we have plotted the flow velocity as a function of the log of height above the bed. Graphically, the roughness height, z_0 , is determined by the $U = 0$ intercept, while the other unknown, u_* , is reflected in the slope of the plot. Note the dependence of the profile shape on both the shear velocity, u_* , and on roughness height, z_0 . The higher the shear velocity (the thicker the flow, the greater the channel slope), the higher the flow speeds at all heights; the higher the roughness, the lower the speeds at all heights.

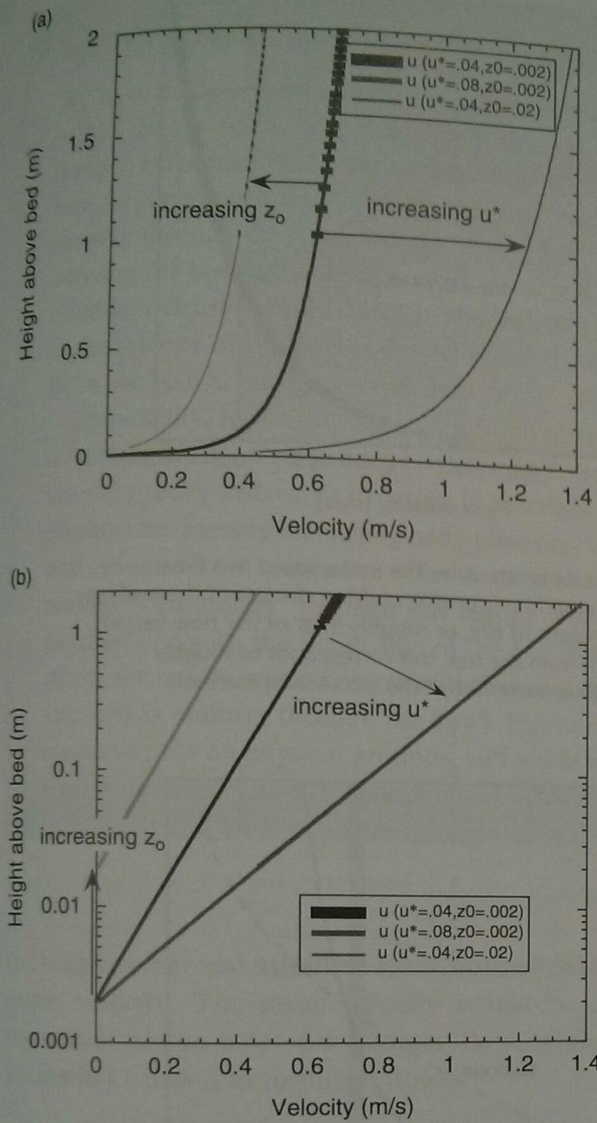


Figure 12.2 Hypothetical mean velocity profiles showing the effects of changes in shear velocity, u_* , and roughness length, z_0 . (a) Linear-linear plot, (b) log-linear plot, on which straight lines represent logarithmic velocity profiles.

A cautionary note: When plotted in this manner, the slope is k/u_* , so that high u_* flows give lower-looking slopes. Remember that these plots are oriented so that one can visualize the flow going left to right, and up on the plot is up in the real world. But mathematically, while the independent variable, z , is traditionally shown on the x -axis, it is shown instead on the vertical.

Why not set $U = 0$ at $z = 0$? Note that we have not used the common assumption that the flow speed goes to zero at the boundary, or the “no-slip” boundary condition that we have used in the case of viscous

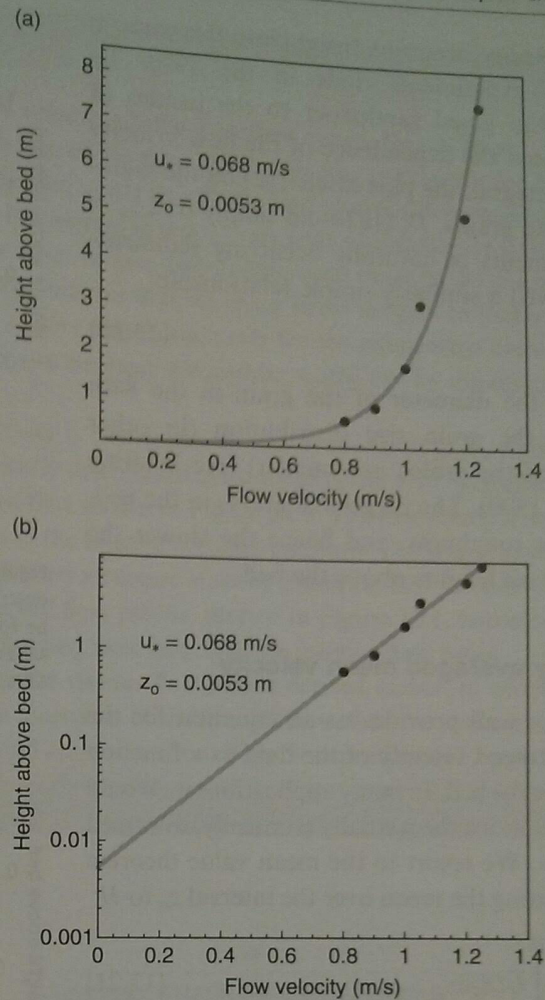


Figure 12.3 Measured flow velocity profiles plotted in both (a) linear-linear and (b) log-linear space. Data from the Mississippi River during the 8 m stage. Flow is well represented by a logarithmic profile with the shear velocity and roughness length shown.

flow developed in Box 12.1. Mathematically, the natural log of zero is undefined, preventing us from setting $U = 0$ at $z = 0$. Physically, the turbulent fluid mechanics that we have assumed breaks down in close proximity to the boundary. In reality the flow becomes viscous as the boundary is approached, and the rheological rule we have used does not apply. But in most channels the region in which this breakdown occurs is very small, of the order of a fraction of a grain diameter.

What does the roughness height, z_0 , mean? We would like to know what about the boundary sets the roughness height. We already know what sets u_* , but, unless we have an expression for z_0 , we cannot

predict the velocity structure. Insight into this came in the form of experiments done in the 1930s by Nikuradse, who glued sandpaper to the insides of pipes, and noted the dependence of the flow velocity (actually its integral, the pipe discharge) on the diameter of the sand grains, D . He found simply that $z_o = D/30$. Experiments in naturally occurring sedimentary beds showed a similarly simple relationship:

$$z_o = D_{84}/10 \tag{12.20}$$

where D_{84} is the diameter of the grain in the 84th percentile of the grain size distribution (in other words, 84% of the grains are smaller) (see Whiting and Dietrich, 1990). The bigger the grains in the bed, the higher the roughness, and hence the slower the flow speeds at all heights above the bed.

The vertically averaged mean velocity

The law of the wall provides us an equation for the temporally averaged velocity of the fluid as a function of height above the bed. In many applications we would like an expression for the spatially (vertically) averaged velocity, $\langle U \rangle$. We resort to the mean value theorem for this, evaluating the mean over the interval z_o to H :

$$\langle U \rangle = \frac{1}{H - z_o} \int_{z_o}^H \bar{U}(z) dz \tag{12.21}$$

Using the law of the wall for $U(z)$, noting that the integral of $\ln(z) = z \ln(z) - z$, and making the simplifying assumption that $H \gg z_o$, yields

$$\langle U \rangle = \frac{u_*}{k} \left(\ln \left[\frac{H}{z_o} \right] - 1 \right) \tag{12.22}$$

This average is shown in Figure 12.4. It occurs well below the mid-point in the flow. We now ask at what level within the flow one should measure this velocity. This would therefore be the appropriate level within the flow at which to measure the velocity, as it would immediately yield the mean velocity, simplifying the calculation of discharge (see below). We simply set the expression for the spatial mean velocity equal to the law of the wall at a specific height, call it z_m , and solve for z_m . The u_*/k cancels out, and we are left with

$$\begin{aligned} \ln(H/z_o) - \ln(z_m/z_o) &= 1 \\ \text{or} & \\ \ln(H/z_m) &= 1 \end{aligned} \tag{12.23}$$

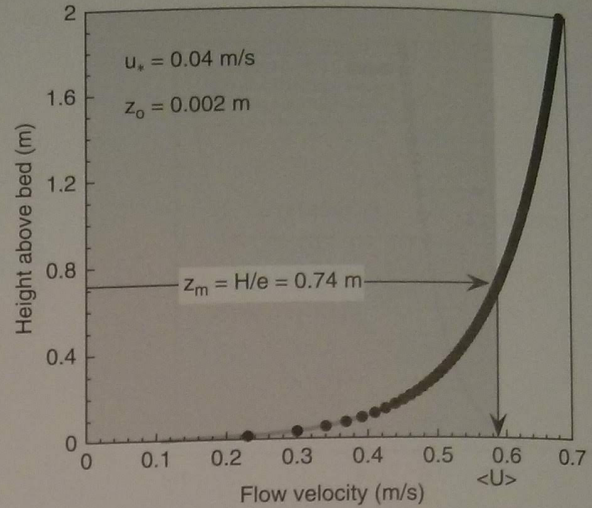


Figure 12.4 The six-tenths rule. The mean speed in a flow described by a logarithmic profile obeying the law of the wall may be found at a height of H/e , or roughly 37% of the flow height. Measured down from the top, this corresponds to roughly 63%, or, rounding, six-tenths of the distance to the bed.

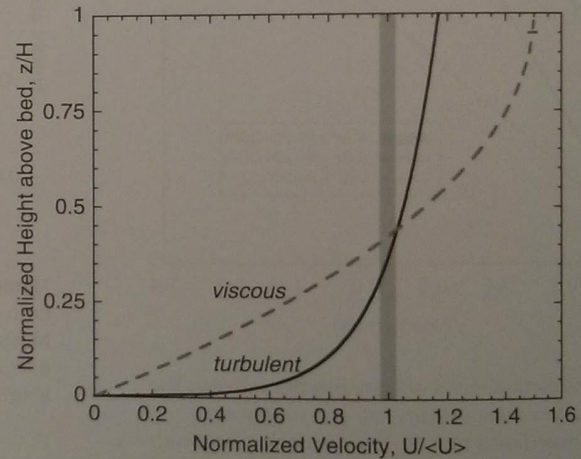


Figure 12.5 Comparison of laminar flow profile with turbulent flow profile, normalized such that they have equivalent mean velocities. The laminar profile is parabolic, while the turbulent profile is logarithmic, and shows much greater curvature near the bed. In both flows the mean speed is found approximately four-tenths of the way from the bed to the top of the flow, or six-tenths of the way from the flow top to the bed.

One more step yields

$$z_m = H/e = 0.37H \tag{12.24}$$

This is the origin of the “six-tenths rule”: the mean velocity will be found at roughly four-tenths (actually 37/100) of the way up from the bed to the surface, or six-tenths of the way down from the surface toward the bed. In Figure 12.5 we show the flow velocity profiles

Box 12.2 A caveat on the mean flow calculation

We have made several assumptions in deriving the flow velocity profile described above. One of these is that the law of the wall holds from the bed to the surface of the flow. While this was convenient for our integral embedded in the derivation of the six-tenths rule, and is not far off, the alert reader will be wondering how we can apply a rheological rule for turbulence that is designed to work "very near a boundary or wall" all the way through the flow, well into the "interior" of the flow. In fact, two assumptions made in the course of deriving the law of the wall break down. First, the approximation that the shear stress is equal to that at the boundary clearly breaks down in the interior. Second, a more appropriate rule for the momentum exchange in the interior of the flow is one in which the eddy viscosity becomes a constant, scaled not by the distance from the bed, z , but by the full flow depth, H .

Empirically, in the interior of the flow, the eddy viscosity is well characterized by $K = (k/\beta)u_*H$, where k is still von Karman's constant ($= 0.4$) and β is an empirically determined constant of about 6.27. The effective viscosity (eddy viscosity) structure is therefore more like that shown in Figure 12.1. The near-bed portion displays the linearly increasing eddy viscosity, while that in the interior becomes constant. The height at which one switches from one to the other description of the viscosity structure is set by requiring that the strain rate remain "continuous" through this region. The resulting full flow profile, plotted in Figure 12.1, becomes a patched one with the log profile of the law of the wall holding near-bed, and the interior flow being characterized by a parabolic profile (in exact analogy to the viscous flow profile derived earlier, in which viscosity is uniform through the flow). But note that the extension of the law of the wall to the surface, while inappropriate on physical grounds, still yields a fairly good approximation of the flow profile, and hence both the mean velocity and discharge based upon it are not greatly altered.

for both laminar and turbulent cases, normalized by the mean velocity. The mean velocity would be found somewhat above $0.4H$ for laminar flow, while it is somewhat below it in turbulent flows.

Other equations for the mean velocity

When attempting to estimate the discharge of a river, it is useful to have a simpler expression for the average flow velocity. These expressions approximate the mean velocity within a channel cross section, which differs from the mean velocity within a vertical profile or the time-averaged velocity at a point.

Manning's equation

One of the more commonly used equations for average velocity in a channel is Manning's equation:

$$U_a = a \frac{R_h^{2/3} S^{1/2}}{n} \quad (12.25)$$

where R_h is the hydraulic radius, S is the slope of the channel, and n is a constant called Manning's roughness coefficient, or Manning's n . The factor a is a

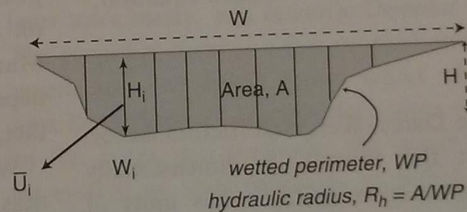


Figure 12.6 Sketch of measurement method endorsed by USGS. The cross section of the channel is broken into many segments, designed such that no more than 10% of the river discharge occurs in any segment. The discharge, Q , is the sum of the discharge in each segment, determined by the product of its depth, H_i , its width, W_i , and its mean speed, $\langle U_i \rangle$. Mean flow equations described in the text utilize the wetted perimeter, and the hydraulic radius of the cross section.

dimensionless constant and takes the value of 1.0 when in SI units, and 1.48 in the English (foot-pound-second) unit system. The hydraulic radius is the cross-sectional area of the flow, A , divided by the wetted perimeter, P , as shown in Figure 12.6. For a roughly rectangular cross section the hydraulic radius is:

$$R_h = \frac{A}{P} = \frac{WH}{W + 2H} \quad (12.26)$$

where W is the channel width and H is the channel depth. For $W \gg H$ (a common geometry) the hydraulic radius is approximately H , the flow depth. The empirically determined Manning's n has been tabulated for a wide range of channel bed and bank characteristics (Barnes, 1967), with values ranging from 0.01 in smooth-walled laboratory flumes to above 0.1 in steep mountain channels. Typical values for natural channels are 0.02–0.08.

The Chezy formula

By analogy to work on flow through pipes, a formula for the mean flow velocity was first proposed by Antoine Chezy in the late 1700s, as he worked on canals in Paris:

$$U_a = C(R_h S)^{1/2} \quad (12.27)$$

where C has become known as the Chezy coefficient, and has units of $m^{1/2}/s$.

Darcy–Weisbach equation

Yet another formula for the cross sectionally averaged flow velocity is the Darcy–Weisbach equation:

$$U_a = \frac{1}{f} (gHS)^{1/2} \quad (12.28)$$

where f is called the Darcy–Weisbach friction factor. Note that at least this formula is dimensionally simple. As the combination $(gHS)^{1/2}$ has units of velocity, the friction factor is dimensionless. As the friction factor increases, the flow speeds at all heights should decline.

The advantage of all three channel-averaged velocity formulas is that all one needs in order to estimate the flow discharge is the cross-sectional area of the flow and this mean velocity. In other words,

$$Q = AU_a \quad (12.29)$$

If one has the relationship between the stage of the flow, and hence its depth H , and the cross-sectional area of the flow, derived from survey information, and calibration to constrain the friction factor or Manning's roughness coefficient, then one can generate an expected rating curve between the easily measured and monitored stage and the more relevant but difficult to measure water discharge.

It is useful to know the relationships between these equations, so that one can move freely between them. Dimensional analysis suggests that we should expect that the mean velocity ought to go as the combination $(gHS)^{1/2}$. One can see that the Darcy–Weisbach formulation starts from this, and that the Chezy formulation comes close to it but neglects to include gravitational acceleration. While Chezy is fine on Earth (and most Parisian canals), this formula could not be exported to conditions on Mars, or on Titan, for example. Manning's formula comes close as well, but is both missing explicit attention to gravitational acceleration, and suggests an extra dependence on H . For very wide flows ($R_h \sim H$), we can rewrite Manning's formula to yield

$$U_a = a \frac{(HS)^{1/2}}{n} H^{1/6} \quad (12.30)$$

to see that the added dependence on flow depth goes as $H^{1/6}$. What about the law of the wall? Recalling that the definition of $u_* = (gHS)^{1/2}$, this formula as well starts from the correct collection of variables. Like Manning's formula, however, the remaining portion of the formula implies additional dependence on H . We can reconcile the law of the wall and Manning's equation by noting that the logarithmic dependence on H/z_o only slowly increases with H . In fact, the dependence looks very much like $H^{1/6}$.

We can now compare the treatments of the roughness or friction coefficients in these formulations, meant to capture the resistance to flow imparted by the bed: z_o , n , and f . For the simple case of a very wide uniform flow, the vertically averaged flow derived from averaging the law of the wall ought to equal a cross-sectionally averaged formula, say the Darcy–Weisbach equation. Setting these expressions equal, and noting again that $(gHS)^{1/2} = u_*$, yields

$$\frac{1}{f} = \frac{1}{k} \left[\ln \left(\frac{H}{z_o} \right) - 1 \right] \quad (12.31)$$

This result suggests that we should not expect the friction factor f to be a constant, but instead that it ought to vary in a specific manner as the flow becomes deeper. In particular, f should decline as the flow thickens. What is important is the ratio of the flow thickness to the roughness height characterized by the size of the grains composing the bed.

Measurement of channel velocity and discharge

Discharge is difficult to measure. It is typically a painstaking and sometimes a dangerous (or thrilling) task. For this reason, we commonly use as a proxy for discharge the stage, or level of the river surface. This can be monitored in a variety of ways, including using a float, or an acoustic sensor. But the easily monitored time series of stage must be transformed into one of discharge through a rating curve. It is the construction of this rating curve that requires we get our feet wet and measure the discharges at a series of known stages.

USGS stream gaging protocol

The formal USGS method of determining stream discharge (Buchanan and Somers, 1969; Wahl *et al.*, 1995), illustrated in Figure 12.6, involves measurement of flow depth and flow speed at each of many "stations" across the flow. More than 20 stations are recommended, such that in no one section is there more than 5% of the water discharge. Measurements are made from a bridge across the flow, or from a cable-car drooped across the river, or on foot by wading into the flow. A station is occupied, and the flow depth is measured (by dropping a large weight to the bed, if done from a bridge). The proper height above the bed ($0.4H$ if a single measurement is being collected) is calculated, and the current meter is placed at this height. The current is usually measured for at least 40 seconds, in order to average out the turbulent eddies that waft by. The product of this mean velocity with the spacing between stations, W_i , and the flow depth there, H_i , yields the discharge of water associated with that portion of the river. The sum of these discharges is the total discharge of the river:

$$Q = \sum_{i=1,n} W_i H_i \bar{U}_i \quad (12.32)$$

Measurement of velocity

We measure velocity using a variety of instruments. Beyond the crudest methods, those practiced by Pooh and Piglet, tossing sticks from the bridge over the river and counting how much time it takes to reach

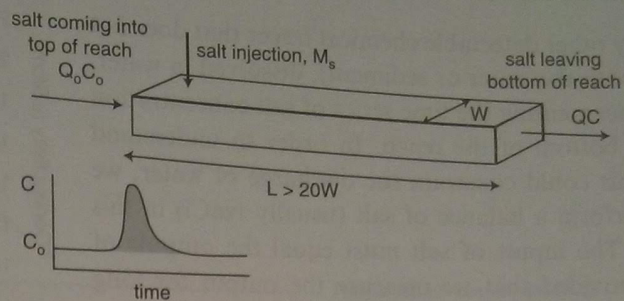


Figure 12.7 Essence of the salt discharge method. A slug of salt of known mass is added to the top of the reach, while the time series of salt concentration, $C(t)$ is measured at the base of the reach chosen such that no discharge is added over the reach, and the distance from the salt injection site is far enough downstream (roughly greater than 20 times the stream width) to ensure that the added salt solution is well mixed.

the other side of the bridge, we use current meters that measure local flow using various technologies. The choice will depend upon the detail with which the investigator needs to know the flow field (for example, is it necessary to know the instantaneous speeds, or is the mean speed at a location sufficient), and the monetary and logistical resources available. These methods include propellor current metering, laser velocimetry, and acoustic Doppler velocimetry. The propellor turns at a rate proportional to the flow speed, and one either counts clicks while listening on a headphone, or records the counts electronically. In the latter two methods, the speed is measured by motion of small particles or bubbles embedded in the flow.

Salt dilution method

If the flow is too gnarly, too complex geometrically, or too dangerous to measure using current meters, one can resort to a chemical tracer method. While in principle this method will work on any flow, its use is limited to relatively small discharges. And while we will describe in detail one such method, this is only one of several methods that have been employed in such situations.

Consider a reach of river chosen so that there are no tributary inputs along the reach. The discharge of water out the base of the reach, Q_1 , therefore ought to equal that into the top of the reach, Q_0 . As sketched in Figure 12.7, the technique entails injecting into the river at the top of the reach a known mass of salt

(or any other detectable chemical tracer that does not react with the water or sediment), dissolved in water, and documenting the time series of salt concentration at the bottom of the reach. In order to understand how this could constrain the discharge of water, we will perform a balance of salt (usually NaCl) in this reach. The inputs of salt must equal the outputs of salt, provided that we measure the output for long enough to ensure that all the salt we injected has had time to make its way to the exit. The balance may be written

$$Q_o C_o T + M_s = \int_0^T Q_1 C_1 dt \quad (12.33)$$

where T is the time over which we have made measurements, M_s is the mass of added salt, and C is the concentration of NaCl in the water (for example, in kg/m^3). Given that we have properly chosen the reach such that $Q_o = Q_1$, we can simplify this equation to yield

$$Q_o = \frac{M_s}{\int_0^T (C_1 - C_o) dt} \quad (12.34)$$

where C_1 is the measured concentration of NaCl in the water at the measurement site, and C_o is its concentration in the incoming water at the top of the reach. We know how much salt we threw into the flow. Therefore all we must measure through time is the time series of salt concentration, from which we subtract a background. Commonly one measures not the salt concentration but the conductivity of the water, which is related to NaCl concentration using a calibration factor. An example of such a measurement is shown in Figure 12.8. The period of integration must extend until the conductivity has returned to the background. The background conductivity in this well-behaved case is steady, allowing simple subtraction, and integration. The final calculation of the water discharge incorporating the calibration of the conductivity probe is

$$Q_o = \frac{M_s}{\alpha \int_0^T (c_1 - c_o) dt} \quad (12.35)$$

where $\alpha = 2140 \text{ (kg/m}^3\text{)/}(\mu\text{S/cm)}$, and the conductivity, c , is measured in micro-Siemens per cm, $\mu\text{S/cm}$.

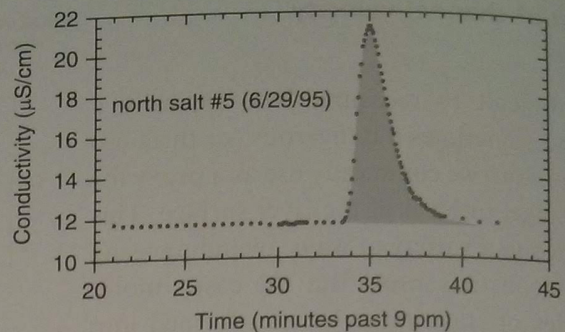


Figure 12.8 Time series of conductivity measured in a small Alaskan glacial stream, from which the water discharge can be calculated. A steady background conductivity was achieved, and measurements were taken for long enough after salt injection to assure that the entire pulse of salt had passed the measurement site. Discharge is calculated from the integral of the conductivity record that rises above the background (shaded).

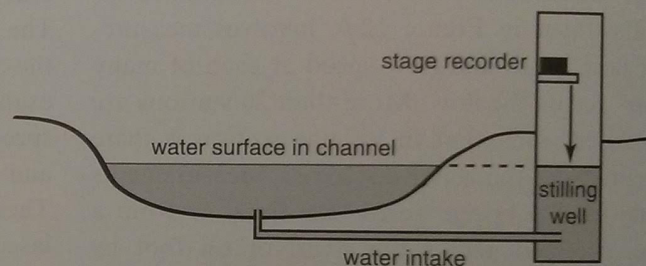


Figure 12.9 USGS stage gaging station. Housing of stage recorder serves as a stable elevation against which water surface level (stage) is measured. Distance from recorder to water surface in the stilling well is measured by a float, a pressure sensor or a sonic sensor.

Measurement of stage

While discharge itself is difficult to measure by one or another of the above methods, stage can easily be monitored continuously. Again a variety of methods have been employed. A staff gage on the bank, or painted on a bridge pier allows easy spot visual inspection. A continuous record of stage is obtained using either a float or a pressure gage in a stilling well, or a look-down sensor such as the acoustic (also called sonic) device. The design of a typical USGS gaging station is shown in Figure 12.9, in which stage is measured continuously with either a float, a pressure gage, or a sonic transducer. While the data streams from these devices were in the past collected on mechanically driven drum recorders, they can now

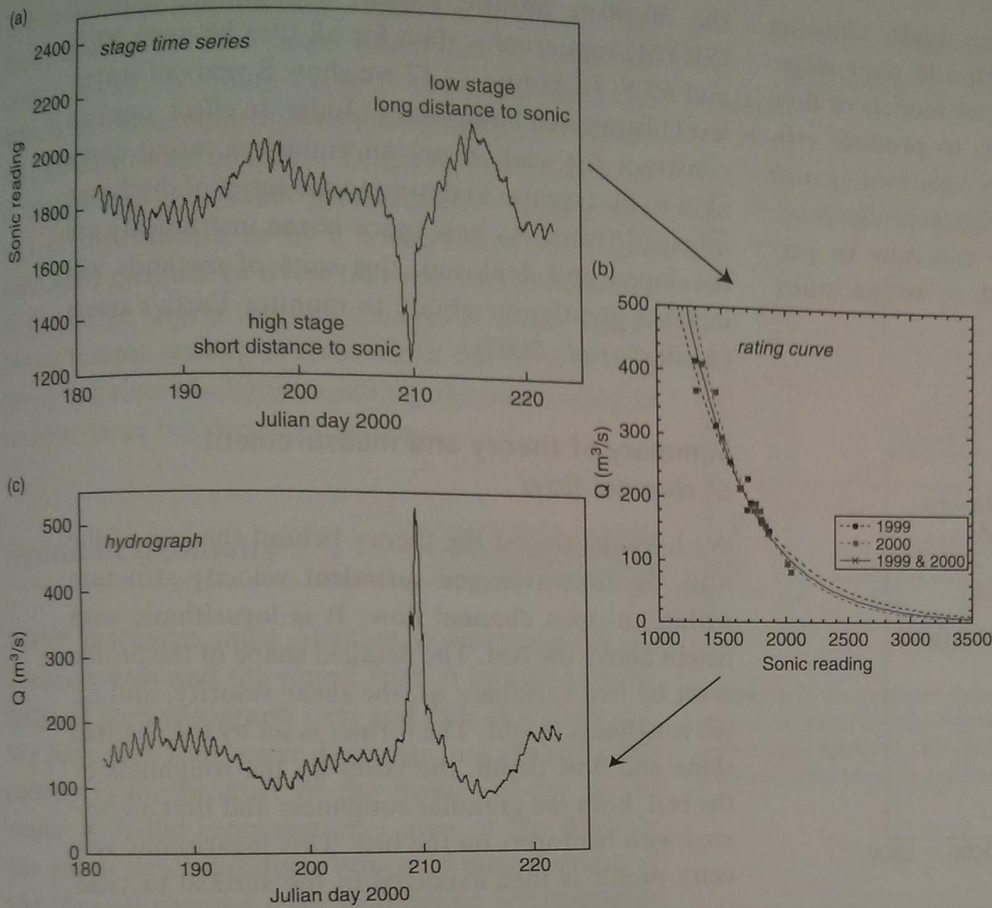


Figure 12.10 Combination of stage time series (a) and rating curve from many discharge measurements (b) to produce hydrograph (c) for Kennicott River, Alaska. Raw readings on sonic instrument are proportional to distance between sonic sensor and river surface. The high stage therefore corresponds to small sonic readings. The rating curve, here shown from measurements made over several summers, shows the expected increase in water discharge with increasing stage (smaller sonic readings). The hydrograph shows the strong pulse of discharge associated with the annual outburst flood from a side-glacier lake.

be logged with a micro-computer. The resulting time series can then be transformed into a time series of discharge using the rating curve, examples of which are shown in Figure 12.10 for the Kennicott River in Alaska.

Space-based measurement of discharge

Finally, we briefly summarize a recently developed method to measure discharge from space (Brackenridge *et al.*, 2005; Smith *et al.*, 1995; 1996; Smith, 1997; see review by Alsdorf *et al.*, 2007). This method, which relies upon orbital remote sensing, is particularly well suited to measurement of rivers in remote areas, and as we will see, is best used in braided river systems. It is straightforward to measure the width of a river from space, as water is easy to distinguish from land surface in a range of wavelengths. If the same reach of a river can be measured repeatedly, one may develop a time series of river width over the runoff season. But we have just seen that a river responds to increases in discharge by widening, deepening, and increasing in

mean speed. How will measurement of width alone suffice? In this simplest application, we rely upon the fact that a braided river maintains a depth such that the shear stress exerted on the channel is roughly uniform, at nearly that necessary to transport the bedload of which the channel is made. In other words, one can safely take $\tau \approx \tau_{crit}$. In order to accommodate more discharge, another braid is accessed, meaning that the effective width of the river increases. As the depth does not increase significantly, the mean speed of the flow also does not change, and the discharge can be written: $Q(t) = H \langle U \rangle W(t)$, where $W(t)$ is the time series of width. In their first application, Smith *et al.* (1995, 1996) turned to braided Alaskan glacially fed rivers to test the method. By comparing space-based width measurements and measurements of the river discharge at constrictions, they showed (Figure 12.11) that the method produced a reasonable proxy for the discharge. Ideally, one could also measure the stage of the river remotely using altimetry data from the satellite. Since then, more sophisticated measurements using other

space-borne instruments have been made, allowing documentation of both river width and river stage. These can be coupled with advanced models of flow in channels and across floodplains to produce estimates of river discharge that can be validated against discharge in specific reaches (e.g., Brackenridge *et al.*, 2005; Smith, 1997). This exercise can now be performed in many areas of the world, as we can utilize

the 30–90 m Shuttle Radar Topography Mission (SRTM) topographic data for all sites between 60°N and 60°S. In Figure 12.12 we show 8 years of water-level history of a large river in India. In effect, one can construct for such rivers an empirical rating curve akin to that we use to develop time series of discharge in gaged rivers. As new space-borne instruments are developed and deployed, this suite of methods will increase greatly our ability to monitor Earth's rivers (Alsdorf *et al.*, 2007).

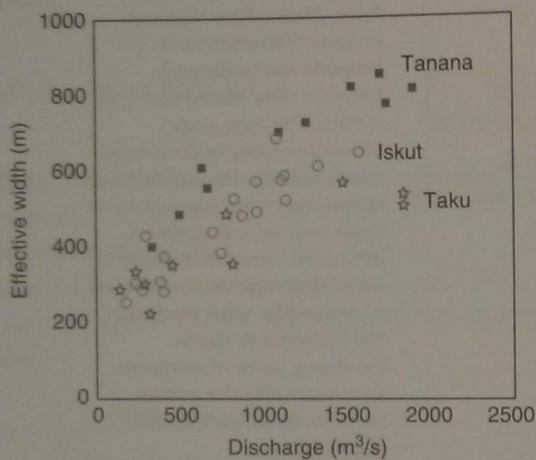


Figure 12.11 Satellite-derived effective channel width and measured river discharge for three braided Alaskan rivers. Each point is determined from a single ERS 1 SAR scene, and the daily mean discharge measured on the date of image acquisition (after Smith *et al.*, 1996, Figure 3, with permission from the American Geophysical Union).

Summary of theory and measurement of channel flow

We have developed the theory behind the law of the wall, the time-averaged turbulent velocity structure within an open channel flow. It is logarithmic with height above the bed. The detailed shape of the profile is set by two variables: u_* , the shear velocity, and z_0 , the roughness height. The former is set by the channel slope and flow depth, the latter by the roughness of the bed, both the granular roughness and that associated with bedforms on the bed. This logarithmic velocity profile is then averaged in the vertical to yield the expected mean velocity, and related to other well-known equations for the mean velocity of a channel. The vertically averaged velocity is found at roughly six-tenths of the way down from the top of the flow, or at roughly $0.4H$. We discussed the means of measuring channel discharge both directly and

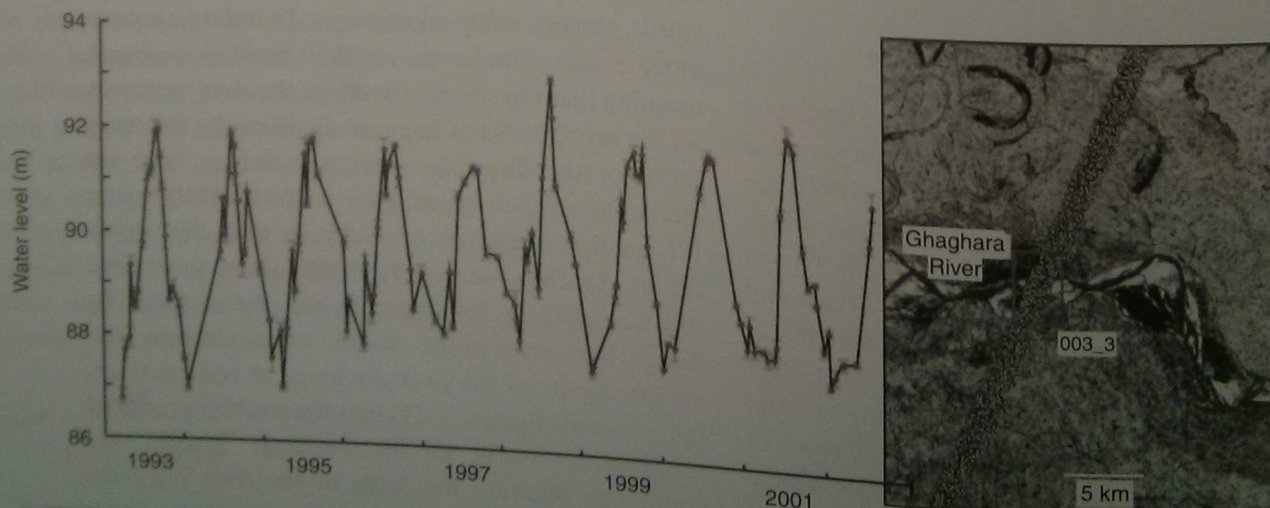


Figure 12.12 Stage history of the Ghaghara River derived from satellite-based measurements (from Alsdorf *et al.*, 2007, Figure 6, with permission from the Nature Publishing Group).

indirectly. Indirect methods require a proxy for the flow, usually the flow stage, which can be measured continuously. A rating curve is required, however, which in turn requires direct measurements of discharge at a range of stages. Direct measurements are accomplished by current measurements using a variety of instruments, or by a conservative tracer (we used salt) method. In rivers that respond to increases in discharge largely through changes in width, spaceborne remote sensing of river width can be used as a proxy for river discharge, enabling the monitoring of remote, large braided river systems.

Hydraulic geometry

Water discharge must increase downstream as the drainage area and the runoff from it increases. Similarly, as the hydrograph rises and falls at a given site. We have seen that water discharge in a channel cross section is the product of the mean velocity of the water with the cross-sectional area of the flow, or the width–depth product. Which of these features of the channel changes most in order to accommodate the need to increase discharge, either downstream at a given moment, or at a site through time? These relationships that reveal how the width, depth and velocity of the flow increase with discharge are called the hydraulic geometry of the river (Leopold and Maddock, 1953). The plots of width, depth and velocity as functions of water discharge, reproduced in Figure 12.13, all show roughly linear trends on log–log plots, implying power-law relationships of the form:

$$\begin{aligned} W &= aQ^b \\ H &= cQ^f \\ U &= kQ^m \end{aligned} \quad (12.36)$$

Note that, since $Q = WHU$, the exponents in the relationships must sum to 1.0: $Q = WHU = ackQ^{b+f+m}$. From the graphs taken from many rivers, Leopold and Maddock deduced that b , f , and m were 0.5, 0.4, and 0.1, respectively. It appears that rivers accommodate additional discharge by equal parts of widening and deepening, with only a little increase in speed. This is perhaps why one can guess with some confidence that a river's speed is about 1 m/s.

In the course of these studies, assembled from the rich USGS gaging data collected over decades of river

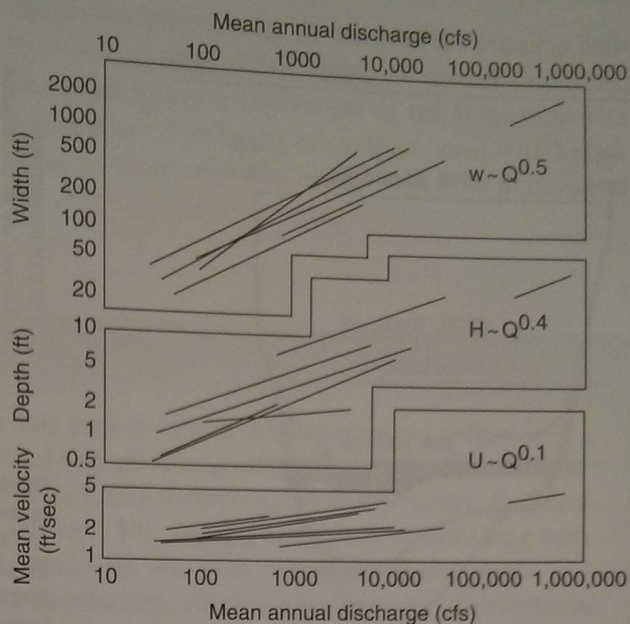


Figure 12.13 Downstream hydraulic geometry of several North American rivers, showing increase of width (top), depth (middle), and velocity (bottom), with increasing discharge downstream (redrawn from Leopold and Maddock, 1953, Figure 9).

monitoring, it was found that these quantities change significantly at a given site. This gave rise to the notion of “at a station” hydraulic geometry. The same relationships yield a different set of powers, implying that the river at a site accommodates changing discharge by changing its shape and speed differently. The values of b , f , and m are 0.26, 0.4, and 0.34. Crudely speaking, the river adjusts all of the available parameters equally. It widens, deepens and speeds up, with the deepening dominating. We have developed the theory for why the river should speed up if it deepens. Given that at any particular site the slope of a river is relatively fixed on the timescales of a single flood event, or over the monitoring period, the speed should increase as the two-third power of depth (using Manning’s equation), or as $H^{1/2} \ln H$ using the law of the wall. The power on the speed exponent should therefore be less than that on the depth, as it is.

Figure 12.14 is a famous plot of channel change during the passage of a flood wave on the San Juan River in Utah. The width changes very little, while the depth of the river changes dramatically. It scours the bed deeply, here by more than 3 m, exposing and entraining sediment stored on the bed of the river. In fact in some of these rivers, including the Colorado

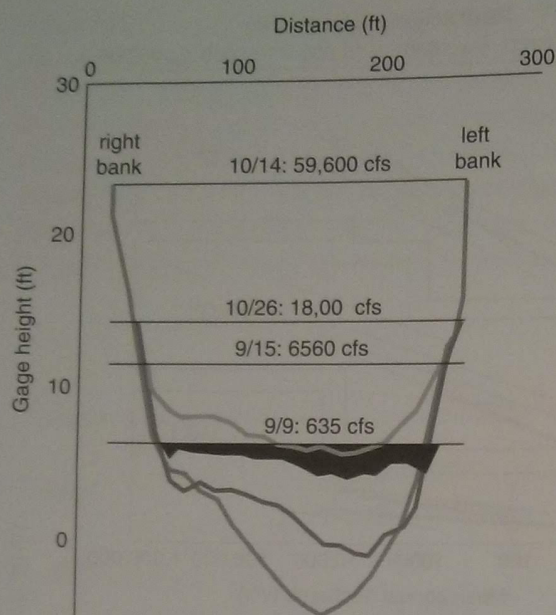


Figure 12.14 Channel scour and re-deposition through the September–December 1941 flood on the San Juan River, near Bluff Utah. Note initial slight aggradation as stage increases, followed by significant scour to depths 10 ft below low-flow bed (redrawn from Leopold and Maddock, 1953, Figure 22).

through the Grand Canyon, the increase in depth due to scour of the bed can equal or exceed the rise in stage during some floods.

These at-a-station hydraulic relationships break down for a braided river, as we have already seen in our discussion of methods for measuring discharge in a braided river. These rivers accommodate additional discharge largely by widening, meaning that the exponent m should be much larger than the others.

Floods and floodplain sedimentation

Our formal treatment of suspended sediment transport provides a quantitative means of assessing the concentrations of various grain sizes at any level in the flow. This is highly relevant to the question of what grains succeed in escaping the channel onto the floodplain, and into the floodplain depositional system in general. When a channel is asked to convey more water than it can convey, the flow extends onto some portion of the floodplain. For planning and zoning purposes, we should therefore consider the floodplain in some sense a part of the channel. The floodplain is simply used less frequently than the rest

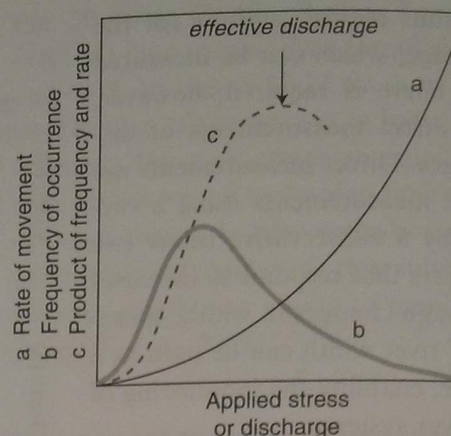


Figure 12.15 The heightened importance of rare events owing to the nonlinearity of the relationship between the applied stress and the sediment movement. The physics of the system controls the relationship between the stress and the resulting geomorphic process rate, (here the curve a), while the climate controls the frequency of occurrence, or the probability distribution of events, curve b. The resulting long-term rate of movement, and the events most important in dictating this long-term rate, are offset from the most common events toward the lower probability, larger events due to the nonlinearity of the physics (redrafted from Wolman and Miller, 1960, Figure 1, with permission from the University of Chicago Press).

of the channel. Overbank flows typically occur every 2–3 years, reflecting the stochastic nature of the meteorological forcing of the fluvial system. Not all years are the same.

Flood magnitudes occur with different frequency, as is captured in Figure 12.15 by the probability distribution of flows. This is one of many examples of the tradeoff between magnitude and frequency in geomorphic systems (see Wolman and Miller, 1960; Costa and O'Connor, 1995). The probability distributions of event sizes tend to be skewed toward the small events; large events tend to be rare (thankfully, and see Chapter 17). On the other hand, the transport of sediment is nonlinearly related to properties of the flow (its depth, its speed, its shear stress). One must sum over all events and the corresponding geomorphic response to the event in order to assess what the total geomorphic response is in the long term, or to assess what might be called the geomorphically significant flow. Graphically, as shown in Figure 12.15, this means that the peak in the geomorphic response curve is shifted toward the larger events than is the peak in the frequency of the events. In the case of the fluvial system, it appears that the channel is naturally designed (meaning adjusted) to accommodate

relatively frequent floods, those that occur on average every 2–3 years (Wolman and Miller, 1960).

The approach advocated by Wolman and Miller in their 1960 work has inspired many to acknowledge the non-steadiness of geomorphic processes. In systems in which flow of some fluid (water, air) incites

the geomorphic activity of concern, for example bedload transport in either eolian or fluvial situations, one must marry a knowledge of the frequency with which flows of differing magnitude occur with knowledge of the relationship between the fluid motion and the sediment transport rate.

Box 12.3 Climate dependence of flood frequency

Using flows documented using the above methods over long periods of time, hydrologists can define the probability of occurrence of flows greater than or equal to a given magnitude. The details of such flood frequency analysis can be found in most hydrology texts or in USGS handbooks. Not surprisingly, the small flows are most frequent, and large flows become increasingly rare. The resulting histograms of flows have been fit with a variety of probability density functions (see Appendix B). The most commonly employed pdfs among hydrologists are the Weibull and Pearson type III distributions, which are asymmetrical distributions with one tail more elongated than the other. The USGS has prepared special probability paper on which a plot of discharge as a function of recurrence interval with a probability distribution of this sort will appear as a straight line. The average annual flood, taken as the arithmetic mean of the maximum instantaneous discharge for all years of record, will plot at a recurrence interval of 2.3 years on such a plot. For many rivers, this corresponds to bankfull flow. In other words, the channel has somehow designed itself to convey the mean annual flood within its banks.

We note that for geomorphic purposes it is the moderate to high end of the flow distribution that counts most, as depicted in Figure 12.15, as these are most capable of transporting sediment, and hence modifying the shape of the channel. The high ends of the histograms of daily flows can in fact be fit quite well with inverse power laws (power laws with negative exponents):

$$p(Q) = \beta Q^{-\alpha} \quad (12.37)$$

This can be seen by plotting not the histograms themselves but the number of days in which the flow of a given size is exceeded, so

$$N(Q) = \sum_i^n (Q_i > Q) \quad (12.38)$$

where N is the number of days the flow on that day, Q_i , has exceeded the flow of concern, Q . $N(Q)$ is the “exceedance probability” of the discharge Q . If the flows are distributed such that the pdf is a negative power law, then the integral of this distribution will also be a power law with a power differing by 1:

$$N(Q) = \int_{Q_{\min}}^{Q_{\max}} \beta Q^\alpha dQ = \left(\frac{\beta}{-\alpha + 1} \right) Q^{-\alpha+1} \quad (12.39)$$

Visualized on a log–log plot, $N(Q)$ should be represented as a negatively sloped line (Figure 12.16) whose slope is $-\alpha + 1$. As the number of days the maximum flow is equaled or exceeded is 1, its exceedance probability is 1 ($= 10^0$). In Figure 12.16, we see that power-law fits capture the essence of the high discharge tails of the distributions, and that the power α differs significantly from catchment to catchment. In general, Molnar *et al.* (2006) showed that the power decreases with aridity, as can be seen by comparing the slopes of the exceedance probabilities from the Arizona (AZ) and Massachusetts (MA) catchments.

In rivers, progress has been made as measurement methods have evolved to document sediment transport. The Helley–Smith bedload sampler (Helley and Smith, 1971) has allowed us to document bedload sediment

Box 12.3 (cont.)

transport rates in a wide range of flows. This kind of data led Andrews (1980) to define the effective discharge, also called the channel-forming discharge, of a river. This can be defined as that water discharge that transports more bedload sediment than any other, averaged over a long period of time. It is formally the product of the bedload discharge rating curve, $Q_{bl}(Q)$, with the probability density function of the discharge, $P(Q)$. Working on the Yampa River in northwest Colorado, he showed (Figure 12.17), as has now been confirmed on many rivers (e.g., Nash, 1994; Emmett and Wolman, 2001), that the geomorphically effective discharge coincides remarkably well with the bankfull stage of the river. In other words, the flows that count most in the formation of a channel are those that fill the channel to its brim. In typical rivers, these occur once every 2–3 years. Those flows that exceed this size flood the floodplain, and occur too rarely to participate significantly in forming the shape of the channel. Those that are smaller, and only partially fill the channel, are too weak to cause significant bedload transport. While others have advocated the use of stream power as opposed to water discharge (Costa and O'Connor, 1995), or have worried about the incorporation of thresholds of motion for various grain sizes in the calculation of effective discharge (e.g., Lenzi *et al.*, 2006), the concept remains the same: one must acknowledge the tradeoffs between the efficiency of a flow and the frequency with which it occurs.

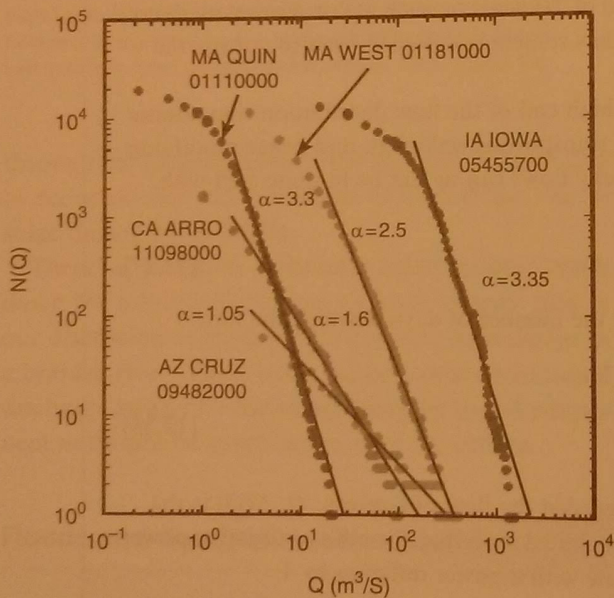


Figure 12.16 Cumulative flow exceedance plots for daily discharge from several US rivers with several decade-long records. The power-law behavior of the high discharge tails to the distributions is indicated by straight line fits to the data, with best-fitting slopes indicated by α . More arid regions (AZ = Arizona; CA = California; IA = Iowa; MA = Massachusetts) display lower slopes (after Molnar *et al.*, 2006, Figure 2, with permission from the American Geophysical Union).

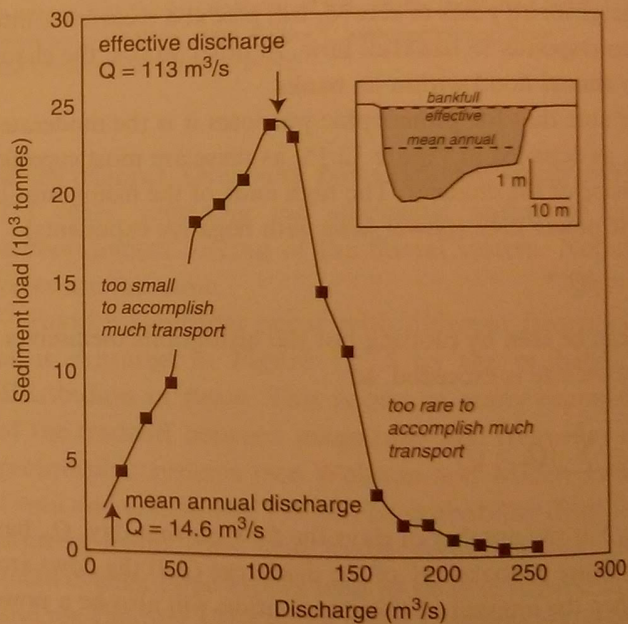


Figure 12.17 Mean annual sediment load transported by increments of water discharge in the Snake River at Dixon, Wyoming. Inset shows channel cross section, revealing how closely the effective discharge matches the bankfull discharge in this river (after Andrews, 1980, Figures 5 and 10 (inset), with permission from Elsevier).

We have seen in our discussion of bedload sediment transport the thresholded nature of the transport, and the nonlinearity of the transport rate above this threshold. This is also seen in data on suspended

sediment discharge, reported in Leopold and Maddock's USGS Professional Paper 252 on hydraulic geometry (Leopold and Maddock, 1953). They argue from assembled sediment discharge data (for example, that plotted in Figure 12.18) that the

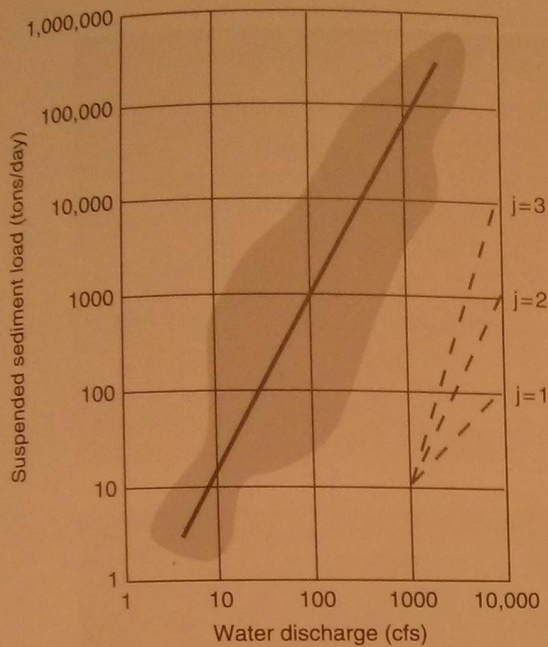


Figure 12.18 Sediment rating curve, Powder River near Arvada, Wyoming. Relationship between suspended sediment load and water discharge; gray cloud encompasses most measurement pairs. This allows calculation of sediment discharge from the more easily known water discharge. A straight line on this plot reflects a power-law relationship, or $Q_s \sim Q^j$. Here j is slightly less than 2 (after Leopold and Maddock, 1953, Figure 13).

sediment load (mass of sediment transported per unit time; they report tons/day) may be related to the water discharge through another power law:

$$Q_s = pQ^j \quad (12.40)$$

The values of the power j are typically between 2 and 3. Again, the system is nonlinear. A flood of double the discharge will transport 2^j , or 4–8 times the sediment. Such assessments for bedload tend to be even more nonlinear, i.e., have yet higher exponents.

The floodplain

Flows that exceed the ability of the channel to convey the water overtop their banks, and flood the floodplain. Overbank flow occurs, also called a flood. The question we may now ask is what sorts of grain sizes are contained in the water that makes its way over the bank? In effect, this water is decanted off the top of the river in the channel, as sketched in Figure 12.19. Consider how the escape of water onto the floodplain will affect its speed. The water slows down because the

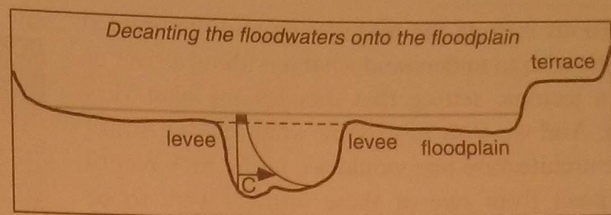


Figure 12.19 Decanting the floodwaters onto the floodplain. Concentration of suspended sediment declines toward the top of the flow, and becomes dominated by fine grains. It is these sediments that are wafted onto the floodplain during overbank conditions.

flow is much less deep, and it experiences drag associated with roughness on the floodplain – grasses, fences, milk trucks, etc. This results in lowering of the ability of the flow to retain particles in suspension. (As discussed in Chapter 14, the relevant non-dimensional number is the Rouse number, which has the shear velocity in the denominator. As the basal shear stress drops because the flow thins, u_* drops, and the Rouse number increases.)

The first grains to drop out of suspension will be the coarser grains decanted off the channel over the banks. These will be deposited locally near the channel banks and lead to the aggradation of the levee. A natural levee is therefore built of the coarsest of the grains that escape the main channel in floods. Those grains that are yet finer will go further on into the floodplain, and will be deposited as the silts and clays that much of the world's fluvial agricultural lands depend upon.

While this is admittedly a simplified view of the floodplain depositional system, the description offered above contains the essence of the floodplain–channel connection. We note that on large rivers water escapes through a set of channels that reverse flow over the course of a flood event, rather than simply in this diffuse overbank mechanism (see the discussion of the Amazon). In addition, as we will see below, it is incorrect to assume that the floodplain is stationary, and that the style of deposition on it will be reflected deeply in the stratigraphy of the floodplain.

Channel plan views

When seen from the air, channels can have many looks, or take on many patterns. The classic

subdivisions include the meandering and the braided cases. We wish to understand what it is about a river or about a tectonic setting that dictates the plan view pattern. And we wish to explore what sets the stratigraphic architecture one would see in the rock record if a deposit from one of these settings were to be preserved.

The braided case

First, consider the braided systems shown in Figure 12.20. Typically, the patterns of braided channels are explained as resulting from situations in which (1) the banks lack cohesion; (2) transport is by bedload only; (3) the flow fluctuates greatly on a frequent basis – perhaps even daily. Braided rivers are commonly found in association with glaciers, as the characteristic glacial outwash channel pattern. The flow occupies two or more channel segments simultaneously, the flow threads separated by mid-channel bars. At times, the flow system can occupy the entire valley cross section, taking up many tens of threads. The mid-channel bars themselves typically lack vegetation, and are composed of usually rather coarse bed material. Flow depths are usually not very great, being at most a few meters.

The lack of fine material and of vegetation leads to the lack of cohesion of channel banks. As the flow depth increases, the shear stress exerted on the bank becomes sufficient to entrain bank material, and the channel widens locally. Note that this is not the case if the channel banks remain intact; such a flow would instead increase in depth. The result is that as soon as the flow becomes deep enough to transport sediment, it begins to widen itself. This limits the flow depths to just greater than threshold depths, i.e., where $\tau_b = \rho g H \sin \alpha \approx \tau_c$. Given that, for a specific reach of stream, we can know the slope, this means the flow depth itself is the only variable.

Interestingly, this means that if we know the slope of a braided reach of channel, and we know the grain size of the bed material, from which we can calculate the necessary boundary shear stress to entrain it, then we can simply use the flow width as a surrogate for the flow cross-sectional area. In addition, we can use theoretical calculations to produce the mean flow velocity to be expected in the flow of critical depth. This means that we can judge the flow discharge in a braided river by

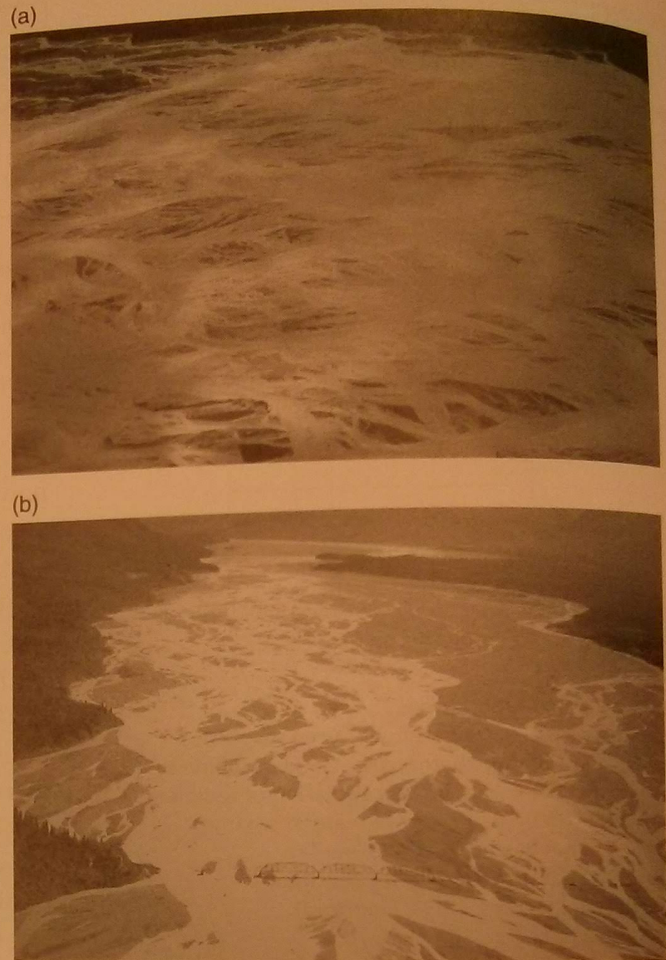


Figure 12.20 Two views of the Chitina River, Alaska, showing extensive braidplain downstream from major glaciers of the Wrangell Mountains. (a) High flow with much of the braidplain occupied by channels. (b) Medium flow, looking up-river, with abandoned train bridge segments for scale (photographs by R. S. Anderson).

summing up the width of the flow across the entire braidplain. This is a fantastic boon, as gaging such a system is essentially impossible, owing to the ephemeral nature of the flow, the mobility of the channel banks (which would have to support the instruments), etc. This method has recently been tested using satellite imagery (Smith *et al.*, 1996), and has been shown to work surprisingly well: width is indeed a very good proxy for water discharge in a braided river as seen in Figure 12.11.

The origin of the braiding behavior has been explored in numerical models (Murray and Paola, 1992), reproduced in Figure 12.21. They find that the dynamism of the system is largely due to flow expansions and contractions, or divergences and

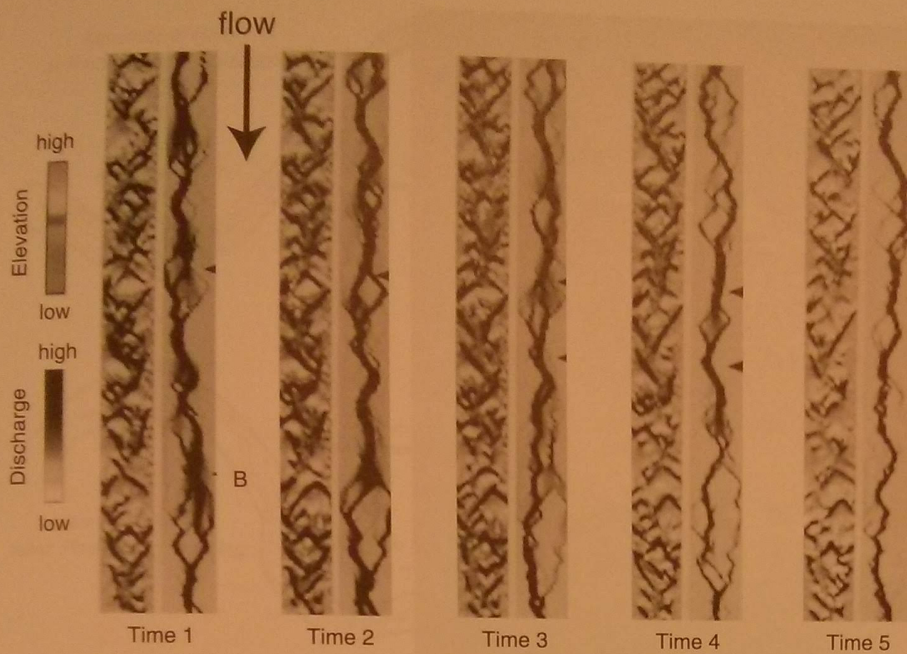


Figure 12.21 Numerical simulation of channel braiding shown at five times, illustrating spatial patterns of both topography (left) and water discharge (right). Mid-channel bar formation at point B is especially instructive to follow through time (after Murray and Paola, 1994, Figure 2, with permission of Nature Publishing Group).

convergences. This in turn sets the divergence of sediment transport, forcing a reduction in sediment transport rate in sites of flow divergence, and an increase in sediment transport over sites of flow convergence. Recalling the erosion equation relating the rate of change of bed elevation to the spatial gradient in the sediment flux, we should expect sites of flow convergence to erode, and sites of flow divergence to deposit. This bed adjustment then changes the local flow, etc. The effect results in a very dynamic set of mid-channel bars, even in the face of essentially steady flow.

You might then ask why braided systems are so commonly associated with highly fluctuating flows. The role of flow fluctuation may relate to the efficient removal of vegetation from the system, which in turn maintains the banks as non-cohesive channel boundaries.

The meandering case

The meandering stream channel pattern is more common. An example is depicted in Figure 12.22. This sinuous snaking of a single-threaded channel is characteristic of all channels that have cohesive alluvial banks (meaning they are composed of river sediment). The sinuosity of a river is expressed as the ratio of the river channel length over the valley

length, and can be many times 1. As shown in Figure 12.23, typical meander wavelengths are very tightly clustered around a dozen (actually 11) times the river width. As you can see in the three maps of meanders at the top of Figure 12.23, this means that in the absence of a scale on the map it is difficult to tell the scale of a river just by looking at a map. River meanders are self-similar.

meander, n. To proceed sinuously and aimlessly. The word is the ancient name of a river about 150 miles south of Troy, which turned and twisted in the effort to get out of hearing when the Greeks and Trojans boasted of their prowess. (Ambrose Bierce (1842–1914), *The Devil's Dictionary*, 1911)

Now that we have paid particular attention to the floodplain and the development of the levee, think for a moment about the channel cross section. Here we ask what determines the stratigraphy in a cross section through the floodplain. Is it composed entirely of floodplain silts away from the channel? At depth, what would one find beneath the silts, and why?



Figure 12.22 (a) Small meandering river on Yukon Flats in interior Alaska. Migration of the meanders is clear from the age (height) of the trees occupying the point bars. Abandoned meanders appear as oxbow lakes to the left of the image, and are clear water because they have no access to the fine sediment being carried by the river. (b) Scroll-bar dominated floodplain in Mississippi Valley. Point bars show as bright white deposits in the interiors of bends. Ghosts of old meander locations are shown in the pattern of the vegetation. Several cut-off meanders appear as oxbow lakes (photograph by R. S. Anderson).

In order to address this question, we have to know something about how meanders work – first how the flow works, and then how the sediment moves through it. Consider a single bend in the river shown in the sketch of Figure 12.24. The flow this time is confined within cohesive banks that are essentially non-eroding on the short timescale of a single flow event. The inside of the bend has a sandy deposit called a point bar that is an active part of the system.

It is unvegetated, and dips gently into the flow. The thalweg, or the deepest part of the flow, is against the far bank on the outside of the bend. In plan view, the thalweg crosses from one side of the river to the next as it passes from one bend to a bend of opposite sign. We might expect the highest basal shear stresses to be associated with this band of highest flow depths. Importantly, the flow field is a complex one and very three-dimensional as it passes through a bend. The

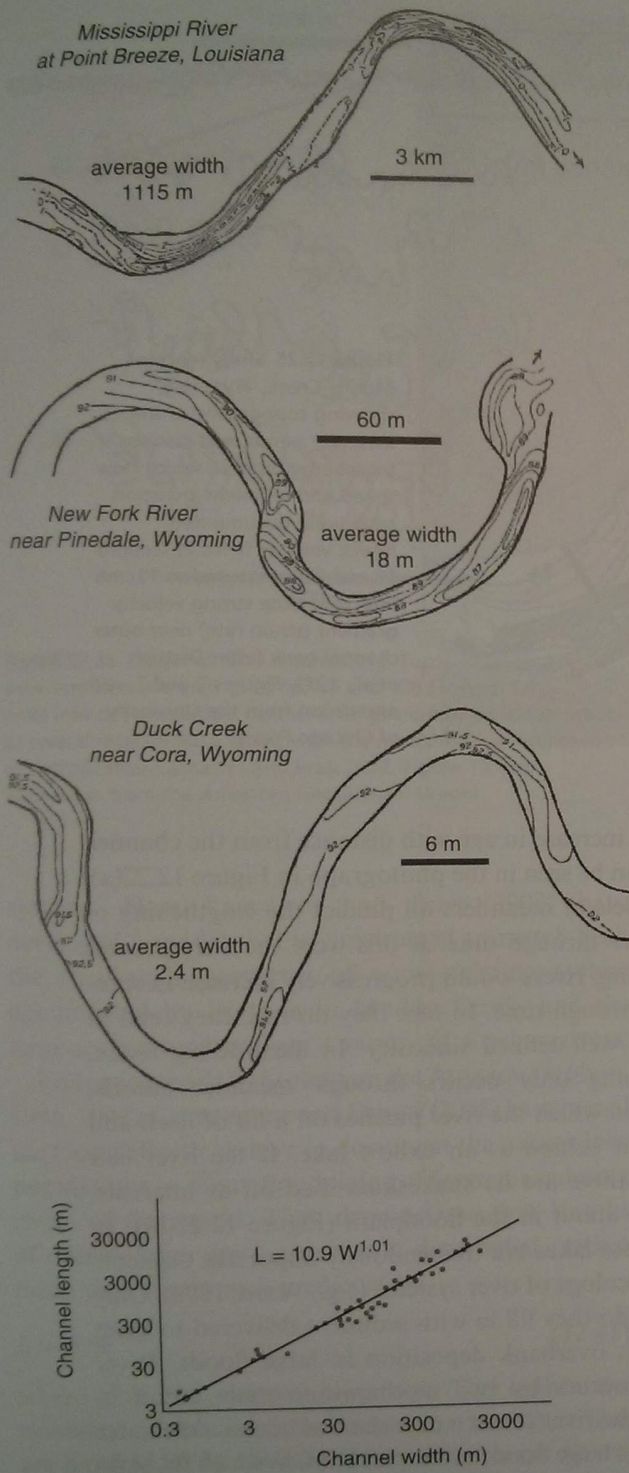


Figure 12.23 Self-similarity of river meanders. Maps: representative meanders from three rivers at scales differing by three orders of magnitude look similar because the radius of curvature and the channel length scale with the channel width. Contours (in feet) show deepenings associated with outer bends in the meanders. Bottom: meander length scales linearly with channel width such that length is roughly 11 times channel width. Open circle is an ice channel (after Leopold and Wolman, 1960, Figure 3 (maps) and Figure 2 (plot)).

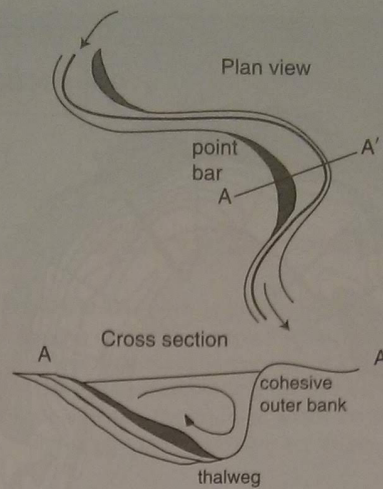


Figure 12.24 Geometry, terminology, and flowfield within a river meander. Super-elevation of the flow on the outside of the bend drives helical flow, which in turn orients the local shear stress inward toward the point bar.

water experiences a centrifugal acceleration as it is made to turn a corner; recall that this goes as the square of the local velocity of the flow divided by the radius of curvature of the bend. As the water high up in the water column has the highest velocity, it experiences the highest outward acceleration. A component of its flow is therefore outward toward the outer bank. This bunches up flow there, and generates a slope on the flow back toward the inside of the bend. This slope produces a pressure gradient that drives flow inward at the bed. All told, this sets up a helical motion of the water as it passes a bend. Now consider the sediment. The shear stress at the bed mirrors the flow immediately above it. On the downstream side of the point bar, sediment is delivered to the point bar through inward motion of grains along the bed, responding to the inward basal velocity of the flow. Those grains small enough to remain in transport out of the main thread will be transported onto the point bar toe, and finer ones will be taken up higher onto the point bar slope. The net effect is a downstream and outward migration of the point bar. Over long timescales, the outer bank is also eroded, as it is there that the highest shear stresses are exerted, as illustrated in Figure 12.25 from the Muddy Creek experiment (Dietrich *et al.*, 1979, 1984; Dietrich and Smith, 1983; Dietrich, 1987). These stresses and the sediment entrainment they allow ultimately result in the erosion of the base of

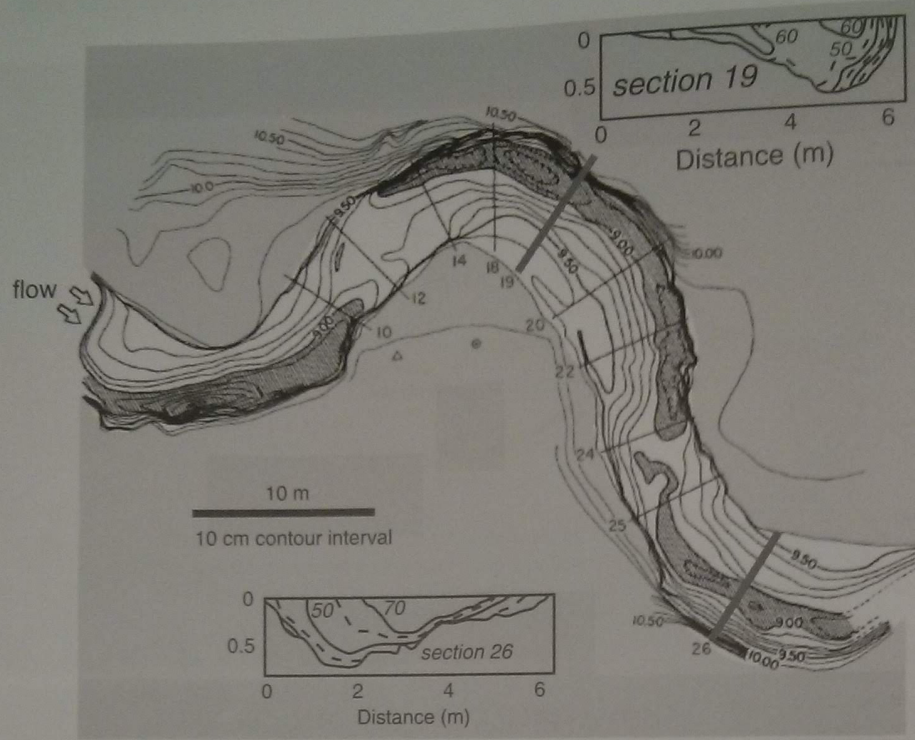


Figure 12.25 Study reach of Muddy Creek, Wyoming, showing topography of the meander bends, and stations (numbered lines) at which flow speed and sediment transport rates were documented. Insets: velocity fields at sections 19 and 26, contoured at 10 cm/s intervals. Note strong velocity gradient (strain rate) near outer channel bank (after Dietrich *et al.*, 1979, Figures 1 and 2, with permission from the University of Chicago Press).

the bank, and cause its failure (see also Hooke, 1975; Smith and McLean, 1984). Over long timescales, then, the meander migrates sideways and down-valley. The back edge of the point bar slowly becomes so inactive that it can be colonized by vegetation, and is left in the wake of the motion of the meander across and down-valley. High floods will ultimately mantle the point bar with overbank deposits. The resulting stratigraphy is a point bar migration deposit, thinly mantled by overbank deposits. Note that the deposit is normally graded – fine grains over coarse grains – as the coarser grains always travel nearest the thalweg of the channel; only the finer grains are carried high onto the point bar before the basal shear stress of the flow drops below their threshold for transport.

The geomorphic expression of a meandering system is one of a plain covered by scroll bars and oxbow lakes (Figure 12.22(b)). The scroll bars mark the migration of the meander through time, and provide strong constraint for the kinematics of pattern evolution (meaning they record the path taken, not the physics of how it happened). One can quantify the rate of meander migration in the short term by comparing aerial photographs of a site. On the ground, we can deduce migration rates by dating the vegetation that colonizes the abandoned point bar; it

should increase in age with distance from the channel. This can be seen in the photograph in Figure 12.22(a).

Models of meanders all predict the lengthening of the river through time. If this were the only process occurring, rivers would progressively increase in sinuosity through time. In fact they do not; they tend to have a well-defined sinuosity. In meandering rivers, shortening only occurs through meander cutoffs, events in which the river pinches off a bit of itself and leaves it behind as an oxbow lake. If the river is a snake, these are its snakeskins shed off at intervals, littered about in the floodplain (Figure 12.22(b)). In fact these lakes are tremendously important elements in the ecology of river systems (e.g., Ward, 1998). Only slowly do they fill in with sediment delivered to them through overbank deposition in large floods. River cutoff occurs by two mechanisms: chute cutoff in which the river forms a new channel across a meander during a large flood, and neck cutoff, in which the slow lateral migration of the planform impinges on itself. Models of meandering rivers (e.g., Howard, 1992, 1996; see also Sun *et al.*, 1996, 2001a–c) demonstrated the importance of the chute cutoff mechanism in limiting the sinuosity of a river. In Figure 12.26 we show the results of a river meander model that illustrates the extremely dynamic nature of meandering

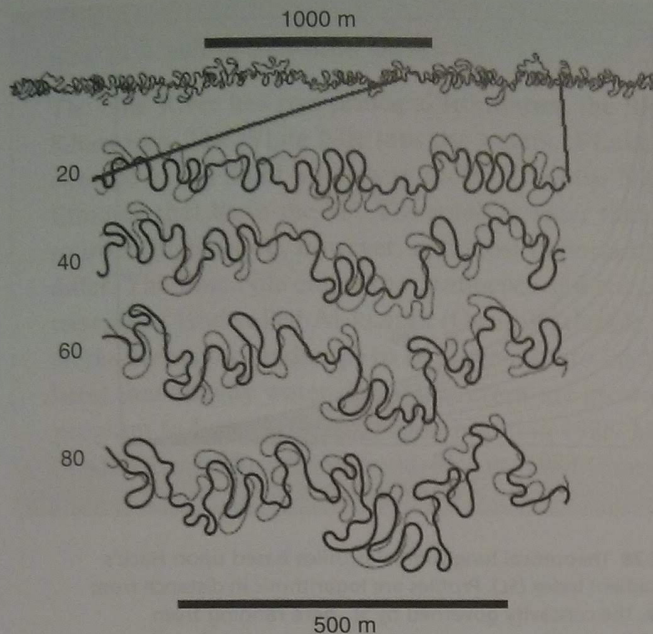


Figure 12.26 Model of river meandering. Top: superimposed channels at 20 (solid) and 100 (dotted) time units into the simulation. Below: enlargement of an 800 m reach at several intermediate times, with the next time superimposed as dotted (after Lancaster and Bras, 2002, Figure 10, with permission from the American Geophysical Union).

systems. Here Lancaster and Bras (2002) have developed a model that is constrained to match both the small-scale geometry of a meandering system documented by Dietrich in Muddy Creek, and the large-scale geometry from a variety of Alaskan rivers.

Following work by Stolum on the Amazon (Stolum, 1996, 1998), Constantine and Dunne (2008) have mined the GoogleEarth archive to document the oxbow lake populations in many floodplains of large meandering rivers of the world. They demonstrate that lengths of oxbow lakes are log-normally distributed, with a mean that is very well predicted by

$$L = 3.0e^{0.82S} \quad (12.41)$$

where S is the channel sinuosity. The higher the sinuosity of the river, the longer are the lakes that are pinched off by the meander cutoff process. Given this empirical rule, they go on to predict the rate of production of oxbow lakes as a function of both the river sinuosity and the rate of lengthening of the river through the meander process. For a steady sinuosity, the rate of river lengthening must balance the rate of loss of river length through meander cutoffs. Highly sinuous rivers apparently lack the

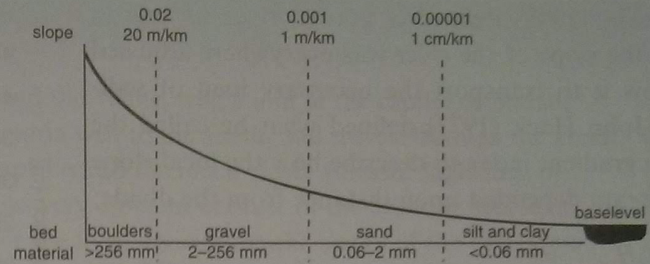


Figure 12.27 Sketch of the longitudinal profile of a river, showing concave up shape. The river here is shown graded to a baselevel that could be the level of a lake or the ocean. The caliber of the sediment comprising the bed declines downstream as the slope declines. The slopes at which the transitions between major grain size classes occur are shown.

efficient chute cutoff mechanism, the physics of which is still poorly understood.

Channel profiles

Alluvial rivers display concave up longitudinal profiles, as shown in Figure 12.27. Channel slopes are steep in the headwaters, and gentle at the mouth. The elevation of the mouth of the river is the baselevel for the river, which is therefore determined by the level of the still body of water into which the river debouches. As this is either a lake or the ocean, either of which can change in level with time, river profiles are significantly affected by temporal variations in baselevel. Changes in baselevel can be either climatically driven, or in the case of the ocean, tidal, or tectonically driven. It is after all the relative sea level that counts to the river. The baselevel can therefore fall due to rock uplift of the land, or rise due to subsidence of the land. Note as well that this change in the vertical would be accompanied by lateral migration of the point at which this baselevel condition is exerted on the river profile. So the bottom boundary condition for a river is dynamic, and can move in both horizontal and vertical position.

The slope of the river must smoothly decline to zero within some small distance of encountering the water body. In turn, this lower boundary condition for the river is felt upstream, generating a “backwater effect” whose length is dependent upon the thickness of the flow and the slope of the flow.

Mackin (1948) defined a graded river as one in which the slope of the river was everywhere adjusted to allow it to transport the necessary load of sediment. John Hack (1973) defined what he called the stream gradient index to describe how the local slope of a stream depended upon distance from the divide:

$$SL = \frac{\Delta H}{\Delta L} L = \frac{\partial z}{\partial x} x \tag{12.42}$$

where the first form is as Hack defined it, and the second is consistent with our terminology. The stream gradient index is in effect a proxy for what is now called stream power (see Chapter 13), or the rate at which energy is made available to do work on the system. If this quantity is roughly uniform throughout the fluvial profile, then we can solve the equation for slope, and integrate to arrive at the expected longitudinal profile of the river:

$$\frac{\partial z}{\partial x} = -\frac{SL}{x} \tag{12.43}$$

$$z = -SL \ln x + C \tag{12.44}$$

where C is a constant of integration. Asserting that the river elevation matches that of baselevel at a distance L from the divide suggests $C = SL \ln L$, which completes the full profile description:

$$z = -SL \ln \left[\frac{x}{L} \right] \tag{12.45}$$

The longitudinal profile is therefore expected to be logarithmic in distance from the divide, as illustrated in Figure 12.28 using a range of slope gradient indices.

The alluvial river profile is concave up, declining in slope with distance downstream. This contrasts with the convexity of hillslopes. We ask here why this is so? In both cases the system must carry more sediment with distance. Recall our arguments for the convexity of hilltops: because in steady state the hillslope discharge must increase with distance, and as most hillslope transport processes increase with slope, the slope must increase. Note also that the hillslope is linked to the stream, which carries away all the sediment. If the stream system is steady as well, the stream too must carry a load of sediment that increases with distance, in fact a load that increases roughly with the drainage area of the basin. As we discuss at length in Chapter 14, the transport capacity of a stream is dependent not just upon the

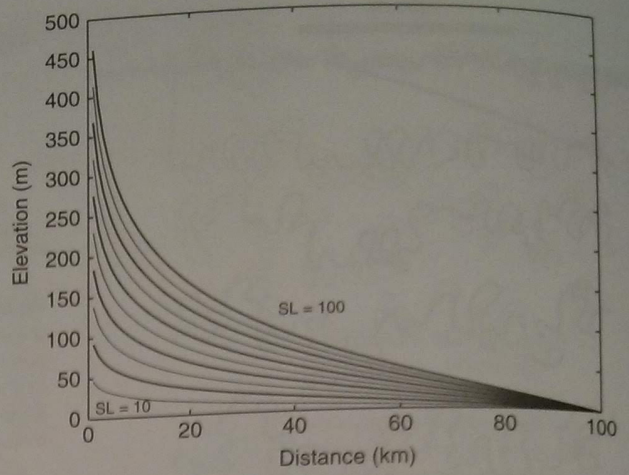


Figure 12.28 Theoretical longitudinal profiles based upon Hack's stream gradient index (SL). Profiles are logarithmic in distance from the divide, the concavity governed by SL , here ranging from 10 to 1000 in equal increments.

slope of the river, but upon the discharge of water. Slope is not all that matters. Another constraint is that the slope of a river surface must vanish as it enters the sea. There is no such boundary condition on the slope of a hillslope.

Let us say for simplicity that the sediment transport goes as the product of the water discharge and the slope of the river, or $Q_s \sim QS$. Let us also assume that the required sediment transport goes as the drainage area of the stream, A^m . If the water discharge also goes as A^m , then $eA^n \sim bA^m S$. Solving for the required S : $S = (e/b)A^{(n-m)}$. As long as $n < m$, the slope will decline with drainage area and hence with distance downstream.

This argument hinges on the capacity of the river to carry the sediment load delivered to it from adjacent hillslopes. Another argument hinges on the competence of a river, or the caliber of sediment it carries. Acknowledging that the mean sediment size on the bed of the river declines with distance downstream (see below), and that the competence of a fluid depends upon the shear stress it exerts on the bed (see Chapter 14), the required shear stress declines with distance. Recalling that the shear stress, τ_b , is ρgHS , the required product of HS declines with distance. We know from downstream hydraulic geometry that the flow thickens with discharge. The required slope must therefore decline with distance; the profile will therefore be concave up.

Box 12.4 White and Blue Niles

The Nile River has two principal tributaries, the Blue and the White, which join in the capital of Sudan, Khartoum. The White Nile taps the waters of Lake Victoria well to the south, and travels through the great swamps of the Sudd on its way north. The Blue Nile taps instead the much closer volcanic highlands of Ethiopia that lie to the SE. The result is water that looks very different because of the differing sediment sources. In addition, however, and most importantly for the local agriculture, the slopes of the two rivers differ. The Blue Nile enters the confluence at a steeper angle. Its water is siphoned to the adjacent edge of the triangle of land called Al Jazirah (Gezira) Triangle, where it then flows gently in a vast complex of irrigation works across the landscape to be taken off into the White at the other edge of the triangle. It is here (and only here) that heavily water-dependent crops are grown in the Sudan. The Gezira Scheme was originally a program to foster cotton farming begun in 1925. More than 10 000 km² is now under irrigation, with wheat production now replacing a third of the land formerly used to grow cotton.

Character of the bed

River beds indeed change in character from their head to their mouth. Some generalizations about changes in sediment size, bed slope, and sediment movement characteristics are outlined in Figure 12.27. The grain size transitions outlined in the figure are commonly seen in rivers, and occur at the channel slopes noted. The two main processes that have been invoked to explain this decline in sediment size are comminution or breakdown of the sediment, and selective deposition of the coarse sediment. Both clearly occur. Sternberg (1875) was the first to propose that the fining could be expressed as a weight-loss function in which the rate of loss of weight of a clast was proportional to the weight. Hence $dW/dx = -aW$, which when integrated becomes an exponential function of distance. The grain weight becomes

$$W = W_0 e^{-x/x_*} \quad (12.46)$$

where W_0 is the original clast weight, and x_* ($=1/a$) is more easily interpreted as the distance downstream the clast must travel in order to decline in weight by a factor of e . This notion became so well ingrained in the engineering literature that it became known as Sternberg's law. Sediment grain size reduction during transport has long been explored experimentally. This began with the extensive work of Kuenen (1956) using drums in which the sediment was tumbled, a method modified by Kodama (1994a,b), and altered altogether by Attal *et al.* (2006) who employ instead vortex flumes. In all such experiments the rate of

decline in grain size is characterized as an exponential with a characteristic travel distance required to reduce grain size by a factor of e . (In the case of drums this was interpreted to be the product of the circumference of the drum and the total number of revolutions.) But Jones and Humphrey (1997) raise another issue. They point out that pebbles and cobbles can rest in an alluvial deposit, say a point bar, for long periods of time between discrete transport events. If during the resting period the clast weathers significantly, the weathered carapace of the clast will be quickly removed once it is again being jostled about during transport. Both physical comminution during transport and weathering during periods of rest ought to produce different rates of size reduction for grains of different rock types or minerals. This lithology-dependent effect has been explored deeply in the work of Attal and Lave (2006) on the Marsyandi River in Nepal, and is discussed further in Chapter 13.

While the grain size of the bed of rivers tends to decline downstream, the decline in grain size can be quite sharp in the case of gravel to sand. The composition of the bed is important for fish habitat, as for example salmon seek gravel beds in which to lay their eggs. This gravel-sand transition can occur over a length of channel that is far too small to be explained by comminution of the sediment. It can occur over a reach of 100 m in small rivers, and over 30 km in large rivers – in both cases a small fraction of the total length of the river. This observation has focused attention on modeling of selective transport



Figure 12.29 A portion of the Gezira scheme irrigation project. (NASA image PIA11079) Inset: satellite image of location of Gezira triangle between the Blue Nile and more gently sloping White Nile.

in a mixed grain size bed. Ferguson (2003) summarizes prior work in his modeling study. He simplifies the problem to two grain sizes, sand and gravel, and is able to reproduce the rapid transition by appeal to the strong dependence of the entrainment threshold on the fraction of the bed that is sand. See Chapter 14 for a detailed discussion of entrainment in sediment transport problems. For a pure gravel bed, the threshold for transport of both sand and gravel is taken to be equivalent. Any sand in the bed is hidden among the gravel particles, and cannot be transported unless the gravel moves. On a pure sand bed, any gravel that exists is highly exposed to the flow, as it sticks well above the sand bed, and therefore rolls freely. Its threshold for entrainment is reduced considerably relative to that on a pure gravel bed. The postulated dependence of entrainment thresholds for gravel and for sand on the sand fraction in the bed results in highly preferential transport of sand at the low excess shear stresses that are characteristic of gravel-bedded rivers. This means that the sand is being transported in greater concentration than it occurs in the local bed, and is therefore winnowed from the bed. This promotes the emergence of a sharp gravel–sand transition, and serves as another example of self-organization in geomorphology.

It should be clear by now that the longitudinal profile of even an alluvial river (not touching down

on bedrock, and therefore immune to the direct affect of the lithology over which it is passing), is quite complex. Because the river has so many features it can adjust to accommodate the need to pass both water and sediment (recall the hydraulic geometry), and because the baselevel conditions for a river are rarely steady for long, there is no simple universal rule for what governs the profiles of rivers. We must acknowledge the details of any particular river, which will include the distribution of area with elevation which in turn governs the distribution of precipitation; the spatial distribution of the sediment supplied to the river, both in quantity and in caliber; the tectonic effects that might include altering the slopes of the river, and the baselevel of the river; and any human influences that might include ponding of water and sediment behind reservoirs, alteration of the hydrographs by land use changes, and so on.

River slopes

The slopes of rivers are quite small. The bigger the river, the smaller is its slope near the mouth. The slope of the Amazon River is of the order of 10^{-5} , or 1 cm/km. This makes large rivers more susceptible to any process that can alter the slope of the landscape. We have touched upon a couple of these in

discussions of geophysical processes in Chapters 3 and 4, including isostatic rebound due to rearrangement of loads on the surface, flow of mantle across the edge of the continent due to large-scale variations in ocean volume, and other tectonic processes.

Take for example the lower Mississippi River depicted in Figure 12.30. The river elevation drops 95 m over the roughly 1000 km distance between Cairo and the Gulf of Mexico, giving it a mean slope of about 9.5×10^{-5} ; the slope appears to decline to about half of this in the following 500 km to Head of Passes as it enters the Gulf of Mexico.

These low slopes also promote switching of the river from one to another course. At times of high sea level as at the present, these large rivers are aggrading near their mouths. If for any reason the river breaches its levee system in these lower reaches, a completely new course down a higher slope to the ocean may be accessed, leading to abandonment of the old channel. The Mississippi has done so several times over the course of the Holocene. In fact, the US Army Corp of Engineers spends a great deal of effort to prevent the Mississippi from occupying the Atchafalaya channel (Figure 12.30), as it is now the steeper route to the ocean. The Yellow River in China (Huang He in Chinese) has jumped from one to another channel naturally as well, entering the China Sea at locations as far apart as several hundred km. The Huang He levees now stand something like 7 m above the adjacent floodplain. Chinese generals have in the past employed the river as a weapon, making use of the low slopes and the extensive floodplains beyond the natural levees. In the latest such event, in 1938 nationalist troops led by general Chiang Kai-Shek dynamited the levees of the Huang He, flooding more than 50 000 km² of the land, and miring the invading Japanese army while killing nearly a million of his own people in the flood.

The influence of baselevel

The baselevel of a river changes with time due to a variety of processes that can change the relative elevation of the land and the sea. Alluvial rivers respond to baselevel changes by sediment infill when baselevel rises, and diffusion of the corner resulting from a baselevel drop. We can understand this by appeal to the equations of continuity of sediment

and of sediment transport. We wish to develop the equation representing the evolution of channel elevation, z . If the substrate is composed entirely of sediment (as opposed to rock), then this equation becomes simply

$$\frac{\partial z}{\partial t} = -\frac{1}{\rho_b} \frac{\partial Q_s}{\partial x} \quad (12.47)$$

where Q_s is the specific discharge of sediment, and ρ_b is the bulk density of the alluvial bed. We now seek an expression for the sediment transport rate. One approach is to use a stream power based argument for sediment transport (see Chapters 13 and 14), in which the sediment transport rate is proportional to the product of the water discharge and the local channel slope. For example, let

$$Q_s = -\alpha Q \frac{\partial z}{\partial x} \quad (12.48)$$

where Q is water discharge, and α is an efficiency coefficient. Combining these results in a diffusion equation

$$\frac{\partial z}{\partial t} = \frac{\alpha}{\rho_b} \frac{\partial(Q \partial z / \partial x)}{\partial x} = \frac{\alpha}{\rho_b} \left[Q \frac{\partial^2 z}{\partial x^2} + \frac{\partial Q}{\partial x} \frac{\partial z}{\partial x} \right] \quad (12.49)$$

In a reach of channel in which water discharge is nearly uniform, the second term in the right-hand side resulting from the chain rule of the derivative drops out, and the equation is more recognizable as a diffusion equation for the elevation of the channel:

$$\frac{\partial z}{\partial t} = \kappa \frac{\partial^2 z}{\partial x^2} \quad (12.50)$$

where the effective diffusivity is $\kappa = \alpha Q / \rho_b$. The sharp corner in the profile generated by the baselevel drop should round more quickly the greater is the sediment discharge, which is scaled by αQ . In Figure 12.31 we show an example of such a case in which the baselevel is dropped at $t = 0$ by 20 m. The corner rounds quickly at first, and more slowly thereafter, and in the long term returns to a stable concave up profile. This style of continuity-based approach is used heavily in models of the filling of basins adjacent to growing mountains, although the details of the transport rule used and the attention to grain size fractions varies between models (e.g., Paola *et al.*, 1992; Paola, 2000).

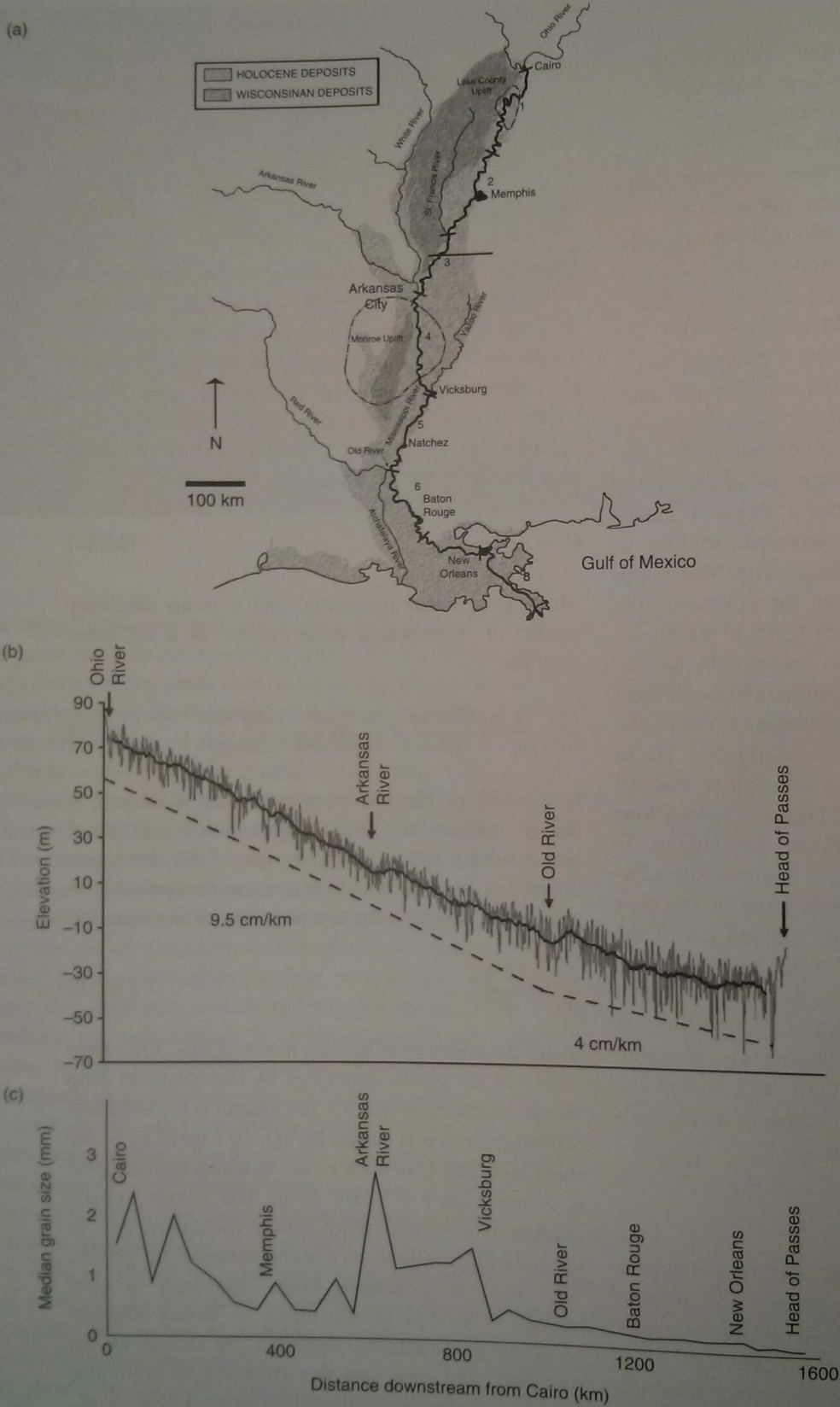


Figure 12.30 Characteristics of lower Mississippi River. (a) Map of lower 1600 km below confluence with Ohio River at Cairo, Illinois. (b) Longitudinal profile, with 40 km sliding mean (bold). (c) Grain size of the bed, showing general decline in median diameter, and influence of major inputs of the Arkansas River (after Harmar and Clifford, 2007, Figures 1, 5, and 9, with permission from Elsevier).

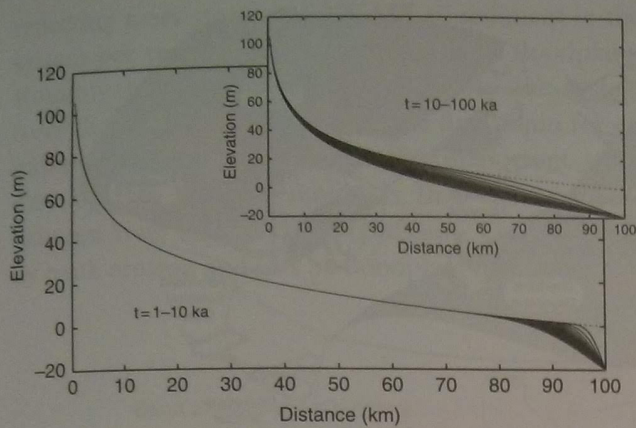


Figure 12.31 Simulations of the effect of a baselevel drop. Diffusive behavior of the system is reflected in the diffusive entrenchment of the mouth of the system. Inset shows long timescale response (1 Ma), demonstrating that the system returns to being concave-up throughout at long times.

The Amazon

We conclude this section with a discussion of the Amazon River, the largest river on Earth. The work we summarize is the product of a decade of research by a team of researchers led by Tom Dunne and Jeff Richey, and aided by many graduate students, among them Leal Mertes (e.g., Mertes, 1994, 1997, 2002; Mertes *et al.*, 1996), Liz Safran (Safran *et al.*, 2005), and Rolf Aalto (e.g., Aalto *et al.*, 2003). The Amazon River is huge by any standard; to take on its study is both important and daunting. As shown in Figure 12.32, the river drains 6.15 million km² of the continent, delivering 6300 km³ of water annually to the ocean (17% of the world's fresh water input) (Table 6.1; after Milliman and Syvitski, 1992). It drains a large portion of the east side of the Andes, and crosses more than 3000 km of the cratonal

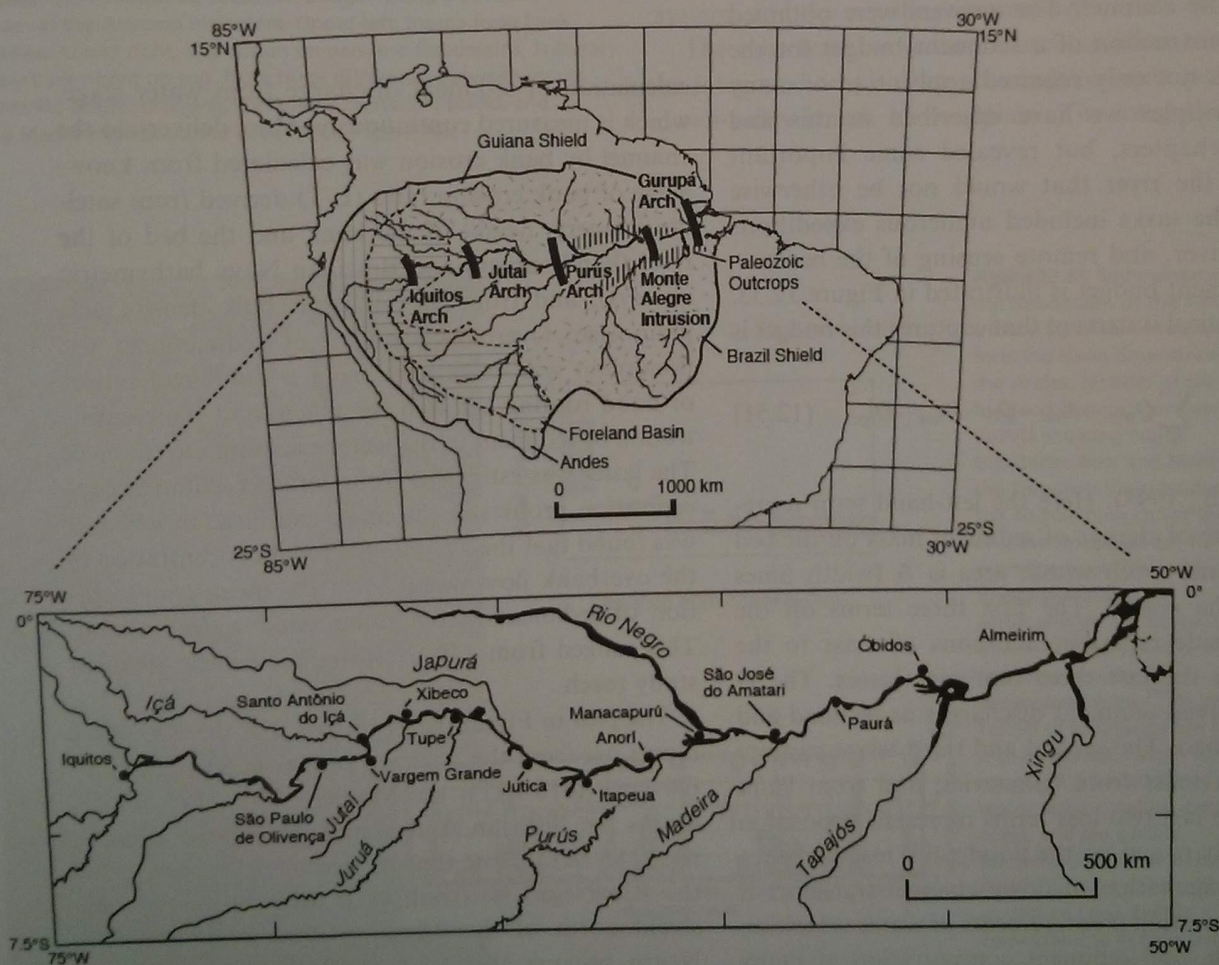


Figure 12.32 Top: map of Amazon River basin, with structural arches, and foreland basin adjacent to the Andean headwaters noted. Bottom: major towns and tributaries of the Amazon (after Dunne *et al.*, 1998, Figure 2).

shield of South America to deliver the water and sediment to the ocean. Its annual flood is so large that it depresses the crust of the Amazon basin by about 10 cm (Alsdorf *et al.*, 2007). The channel slope is so low (2 cm/km) that it is very difficult to measure accurately. Water depths are measured in tens of meters, and the channel widths in the mainstem are 2–4 km. Roughly 1200 Mt (megatonnes, or 10^9 kg) of sediment reaches the Amazon delta each year, delivering roughly 20% of the world's sediment supply to the ocean. Assuming a bulk density of sediment of roughly 1700 kg/m^3 , this corresponds to 0.7 km^3 of sediment volume delivered to the ocean each year.

The questions posed in this research include: How does this sediment reach the coast? Where does the sediment come from, and how long does it linger in floodplains as it passes through the system? Is there net storage in the floodplain? How much sediment exchanges between the floodplain and the channel? The answers were obtained through construction of a sediment budget for the river, which not only required application of many of the principles we have described in this and preceding chapters, but revealed some important aspects of the river that would not be otherwise obvious. The tasks included numerous expeditions down the river, and remote sensing of the basin.

The sediment budget is illustrated in Figure 12.33. A mathematical statement that captures this budget is

$$\frac{\partial(\rho_b Az)}{\partial t} = Q_u + \sum_i Q_{\text{trib},i} + E_{\text{bk}} - Q_d - D_{\text{bar}} - D_{\text{fpc}} \quad (12.51)$$

(Dunne *et al.*, 1998). Here the left-hand term represents the rate of change of sediment mass on the bed of the channel reach whose area is A (width times length of the reach). The first three terms on the right-hand side represent additions of mass to the reach, while the last three represent losses. The Q terms are fluvial sediment discharges as bedload and suspended load. The second and third terms capture additions of mass from tributaries, and from bank erosion. The last two loss terms represent deposition on channel bars and on the floodplain, respectively.

The documentation of down-channel transport is accomplished using measurements of water velocities, depth, width, and sediment concentration at many stations in the river at a variety of stages. From these one can construct sediment rating curves that allow

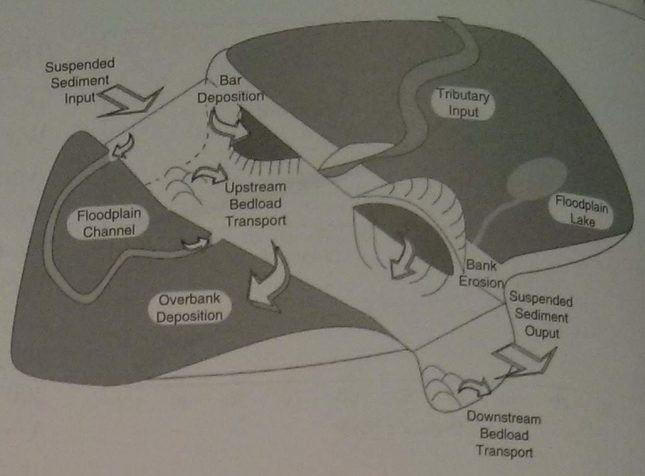


Figure 12.33 Sediment budget for a reach of channel and adjacent floodplain. The budget must account for sediment delivered to the channel from upstream, from tributaries within the reach, and from bank erosion. It may leave the reach by transport in the channel, deposition on bars, through diffuse overbank flow, and through floodplain channels (Dunne *et al.*, 1998, Figure 1).

calculation of sediment discharge from water stage, which is measured continuously. Mass delivery to the channel by bank erosion was calculated from knowledge of bank erosion rates (L/T) derived from satellite imagery, height of the bank and the bed of the river (hand surveys and Brazilian Navy bathymetric surveys), and from the sediment bulk density and grain size. Overbank delivery of sediment to the floodplain was calculated using a numerical model of flood routing through the reach, and the concentration of sediment in the water escaping the channel. The latter was estimated from detailed sediment concentration profiles in the mainstem flow, in which it was found that the average sediment concentration in the overbank flow was 0.33 of the mean concentration of sediment in the channelized water column. This ranged from 140 to 80 mg/L over the 2000 km study reach.

The plot in Figure 12.34 reveals that the dominant inputs are from the Amazon proper at Sao Paulo de Olivenca (616 MT), the Madera (715 MT), which drains the Bolivian Andes, and the smaller tributaries (117 MT). Note that the sediment delivery from the Rio Negro is trivial, as it drains the low-relief shield north of the Amazon; it is called the Rio Negro because the water is black, largely due to its high organic content. The output at Obidos (1239 MT) is less than the sum of these inputs,

reflecting a net storage of 209 MT of sediment in the system per year, most of which is on the floodplain. Roughly 14% of the sediment input to the system from the tributaries is stored in the floodplain for an unknown period of time. Another important story told by this budget exercise is that the exchange between river and bank is significant. Gain of mass by bank erosion and loss by floodplain deposition (up

and down arrows in the diagram) is of the same order of magnitude as the channel transport. This aspect of the budget also implies that the sediment that makes its way out of the system toward the ocean at Obidos will likely have spent time in the floodplain. The pipe of the Amazon is very leaky. During storage on the floodplain, chemical weathering can act to alter the size and mineralogy of the sediment.

In fact, in a companion study, Aalto *et al.* (2003) have discovered that the delivery of sediment to the floodplain of the Amazon is quite episodic. Their data, reproduced in Figure 12.35, suggest that only about one in eight years leaves any record at all, and this record is represented by many centimeters of sediment. The authors attribute this pulsed nature of deposition to la Niña portion of El Niño/Southern Oscillation (ENSO), which brings tremendous rainfall to the headwaters of the Amazon. Once again, we see the operation of a nonlinearity of the geomorphic system, and the resulting importance of rare events.

The time series of sediment accumulation rate can be integrated to yield an accumulation rate per unit down-valley length of floodplain. The integral of an

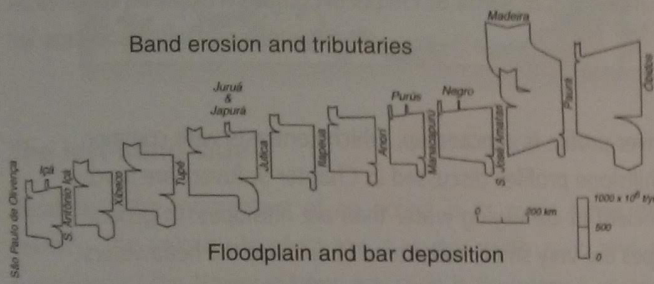


Figure 12.34 Measured sediment budget along a 2010 km reach of the Amazon mainstem. Upper left: inputs from bank erosion. Lower right: deposition on bars and floodplains. Tributary inputs are noted on top. Note huge difference between inputs from Rio Negro, draining the Guiana crystalline shield, and Rio Madeira (after Dunne *et al.*, 1998, Figure 10).

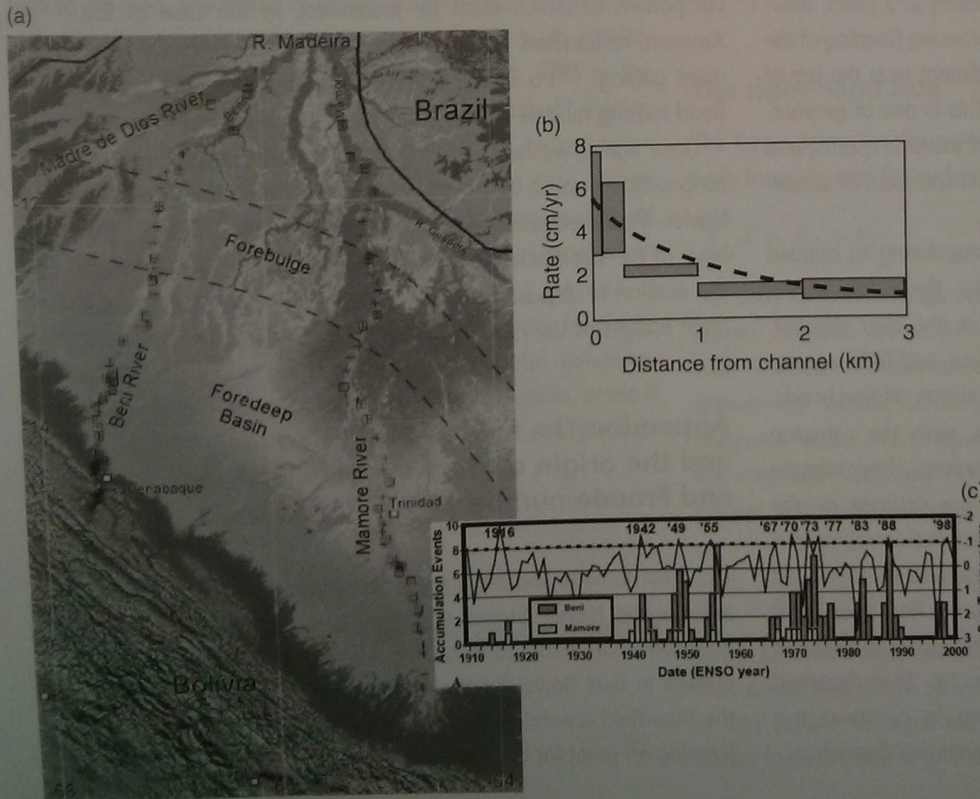


Figure 12.35 Sedimentation on the floodplains of the Amazon tributaries as they cross the foreland basin downstream of the Andes. (a) Map of the foreland basin in northern Bolivia showing major tributaries Beni and Mamore, the foredeep basin loaded by the encroaching thrust sheets, and the forebulge yet further from the load. Transects of floodplain sediment accumulation are shown in boxes. (b) Average rate of sediment accumulation determined from ²¹⁰Pb profiles. Falloff of sedimentation rate has a characteristic length scale of roughly 1.5 km. (c) Dates of major sedimentation events in cores, and sea surface temperatures in the eastern Pacific (la Niña threshold shown as dashed line). Events correspond to la Niña events (after Aalto *et al.*, 2003, Figures 1–3, with permission from Nature Publishing Group).

exponential is simply the value of the y -axis (here 5 cm/yr) with the characteristic length scale (here 1500 km). The authors calculate that the rate of storage on the floodplain of the Beni tributary is 100 Mt per year.

The measurements and synthesis of them that we have presented here represent roughly 20 years

of effort on the part of a large group of researchers. The result is that the Amazon River now serves as an example of how one should conceptualize a geomorphic problem as a budget, here of sediment, which in turn dictates what must be measured.

Summary

Rivers are dynamic components of the geomorphic transport system, delivering water and sediment to the oceans. They are self-organizing features of the landscape, constructing their own channels to accomplish these assigned tasks. Early in this chapter we introduced the mechanics of turbulent flow profiles, and reviewed the means by which river discharge is measured.

Rivers respond to water inputs from the landscape (hillslopes) and from glaciers in the headwaters. Given the stochastic nature of the water delivery system, which is ultimately dictated by the many scales of variability in the atmosphere discussed in Chapter 5, the peak flows transported down the river differ from one year to the next. A typical meandering river self-designs a channel capable of carrying most of these flows. Every 2–3 years, however, flows exceed the channel's capacity, causing flooding of the floodplain, and transport of the finest sediment near the top of the flow outward across the floodplain. This is one of geomorphology's greatest examples of the role of extreme events, and illustrates the need to acknowledge the full spectrum of atmospheric inputs to which a river is subjected.

The bestiary of rivers ranging from meandering to braided plan views reflects the variability of flows, the nature of the sediments involved, and the vegetation in the river corridor. Braided forms reflect high variability of flow, and little vegetation. They respond to increases in flow by simply adding braids. Meandering rivers have cohesive banks, with the cohesion commonly arising from roots of vegetation. They migrate toward their outer banks, leaving point bar deposits on the inner banks, which in turn leads to a characteristic stratigraphic architecture. Floodplains are commonly capped by the finest components of the suspended sediment as the flow goes over-bank in a flood. We develop the quantitative tools to evaluate suspended sediment profiles in Chapter 14. This decanted sediment falls first on the levee, helping to construct this important natural separator between channel and floodplain.

The river profile is concave up, which contrasts with common convex hillslope profiles discussed in Chapter 9. Rivers are much more efficient at conveying water than are hillslopes. In general their slopes are very small, order tens of m/km in the headwaters and as low as cm/km near their mouths. The river comes to zero slope at its baselevel – at its junction with the bounding body of water, the ocean or a lake. Alluvial rivers are continually adjusting to changes in the baselevel. Large rivers have slopes small enough that they are vulnerable to even the broad scale geophysically driven tiltings of the land we have discussed in Chapter 3.

We have seen in the work on the Amazon that even large alluvial rivers can be treated as having sediment budgets, each component of which must be measured. In the case of the Amazon, researchers have combined classical water and sediment gaging, ^{210}Pb dating of sediments, remote sensing and flood routing models to constrain these components.

Once again, we have employed the organizing principle of continuity in several of the analyses: in the development of the Navier–Stokes equation (see the appendix to the chapter), the basis of the salt-discharge measurement of flow measurement, the erosion or deposition of an alluvial bed, and in the sediment budget of the river as a whole.

Appendix: The Navier–Stokes equation and the origin of the Reynolds and Froude numbers

The most famous and most important equation in fluid mechanics is the Navier–Stokes equation. It is application of this equation that leads to solutions for the expected velocity profiles in lava flows, for the discharge of fluid in a pipe, for the flow-field around a settling grain in a fluid. It is also the jumping off point for derivation of velocities in a turbulent fluid.

The Navier–Stokes equation is a highly embellished version of Newton’s second law, which states that the rate of change of momentum of an object is the sum of the forces acting on that object. You are no doubt familiar with the form $F = ma$, where F stands for the sum of the forces, m the mass of the object and a its acceleration. Our first task is to rewrite this in a form that better reflects the words:

rate of change of momentum = sum of forces

As usual in these derivations, we expect to arrive at a differential equation reflecting these words.

The left-hand side

Recall that the momentum of an object is its mass times its velocity. The velocity is of course a vector, with x , y , and z components. The Navier–Stokes equation is therefore a vector equation. We will develop here one of the three components of this equation, the x -component. Once this is developed, the other two components can easily be written. Here as usual we will take the object to be our control volume, or box of fluid, with sides dx , dy , and dz . If ρ is the density of the fluid, and u is the velocity in the x -direction, the x -component of the momentum is then $\rho u dx dy dz$. We must make a strategic decision about how to proceed. The frame of reference in Newton’s case is the object itself: when following along with the object, its acceleration is the sum of the forces acting upon it. This is the Lagrangian frame of reference. If we allow our box of fluid to move about, we are in this frame. If it is held still, tacked down in space, we are in the Eulerian frame of reference. One can get between the two, but one must decide which frame to operate in as we proceed with the derivation. We will choose to work in the Lagrangian frame for now. This means that the rate of change of momentum must be written as if we are following the fluid. The derivative used in this case is the total derivative, or the material derivative, or the substantial derivative, or most informatively, the derivative following the parcel. So the left-hand side becomes

$$\frac{D(\rho u dx dy dz)}{Dt} \quad (12.52)$$

where D/Dt is the total derivative operator, and is a shorthand for four terms:

$$\frac{D}{Dt} \equiv \frac{\partial}{\partial t} + u \frac{\partial}{\partial x} + v \frac{\partial}{\partial y} + w \frac{\partial}{\partial z} \quad (12.53)$$

The first of these reflects the acceleration at a point, holding x , y , and z constant. The other three terms are called advective terms, and represent the advection of momentum, here the x -component of momentum. The mathematical signature of an advective term is that it has the form of $u(dA/dx)$, where u is the component of velocity in the x -direction. The quantity A could be anything: concentration of heat (temperature), concentration of momentum, concentration of fish . . .

While we can easily factor out the volume of the parcel, $dx dy dz$, from Equation 12.52, we cannot easily separate the density from the velocity. We must chain rule each of the four terms that the total derivative represents. After some rearrangement, this yields

$$dx dy dz \left[\rho \left(\frac{\partial u}{\partial t} + u \frac{\partial u}{\partial x} + v \frac{\partial u}{\partial y} + w \frac{\partial u}{\partial z} \right) + u \left(\frac{\partial \rho}{\partial t} + u \frac{\partial \rho}{\partial x} + v \frac{\partial \rho}{\partial y} + w \frac{\partial \rho}{\partial z} \right) \right] \quad (12.54)$$

or

$$dx dy dz \left[\rho \frac{D(u)}{Dt} + u \frac{D(\rho)}{Dt} \right] \quad (12.55)$$

Note that, in the incompressible case, the total derivative of density is zero, and the second term vanishes.

The right-hand side

The forces acting on this parcel of fluid come in two flavors: the body force, F_b , and the surface tractions, F_t :

$$\sum F = F_b + F_t \quad (12.56)$$

The body force acts on the center of mass of the fluid, while the surface tractions act on the sides of the body. The body force with which we are concerned in geomorphology is that due to gravity: the weight of the parcel. (The other body force is magnetic force.) The component of the fluid weight acting in the x -direction is simply the mass of the fluid times the component of the acceleration due to gravity in the x -direction, g_x , or

$$F_{bx} = \rho dx dy dz g_x \quad (12.57)$$

It will be this component of gravity in the downslope direction that drives flow down an inclined plane.

The surface tractions are harder to deal with. These come about from the action of one element of the fluid on another,

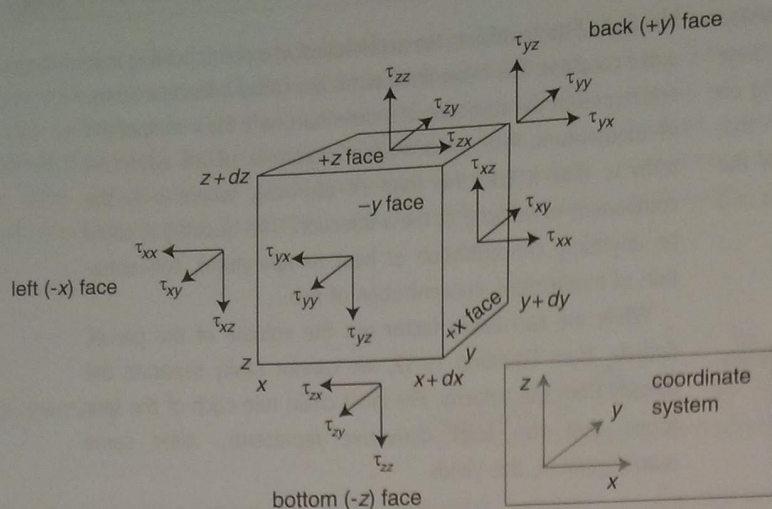


Figure 12.36 Definition sketch for system of stresses acting on a central volume. All stresses are positive as shown.

pushing or pulling it, or shearing it. The problem is that we have to recognize that these fluid forces act in directions that are both normal to a surface and tangential to it, and they act on all faces of the box. In other words, we have two directions to keep track of: the face on which the force is acting, and the direction in which it is acting. First, recall that a force is a stress times an area, in other words, a stress is a force per unit area. We are eventually going to sum up all the forces acting in the x -direction. Each of these forces will consist of the product of a stress times the surface area of the face on which the stress is acting. To be organized about this, we will obey the sign convention depicted in Figure 12.36, in which all of the stresses are depicted as positive. Normal stresses are taken to be positive in tension, in other words when they are directed away from the body. Shear stresses are taken to be positive when they act on the "downstream" face of the box, and are acting in the positive x -, y -, or z -direction. For example, the normal force acting on the left face of the box, in the x -direction, is the normal stress, $-\tau_{xx}$, where the minus sign reflects the fact that the stress as shown is acting in the negative x -direction, times the area of the side of the box, $dydz$.

The sum of the surface forces acting in the x -direction is then

$$F_{ix} = -\tau_{xx}(x)dydz + \tau_{xx}(x+dx)dydz - \tau_{yx}(y)dxdz + \tau_{yx}(y+dy)dxdz - \tau_{zx}(z)dxdy + \tau_{zx}(z+dz)dxdy \quad (12.58)$$

There is one term for each of the six faces of the fluid element. Dividing this expression by the fluid volume $dxdydz$, and recognizing that there are three pairs of terms that reduce to derivatives in the limit as we shrink dx , dy , and dz to zero, allows us to collapse the full force balance equation to

$$dxdydz \left[\rho \frac{Du}{Dt} + u \frac{D\rho}{Dt} \right] = dxdydz \left[\frac{\partial \tau_{xx}}{\partial x} + \frac{\partial \tau_{yx}}{\partial y} + \frac{\partial \tau_{zx}}{\partial z} + g_x \right] \quad (12.59)$$

Dividing through by the mass of the fluid element, $\rho dxdydz$, and assuming that the fluid is incompressible ($D\rho/Dt = 0$), yields a general equation for a force balance in the x -direction of an incompressible fluid:

$$\frac{\partial u}{\partial t} + u \frac{\partial u}{\partial x} + v \frac{\partial u}{\partial y} + w \frac{\partial u}{\partial z} = \frac{1}{\rho} \left[\frac{\partial \tau_{xx}}{\partial x} + \frac{\partial \tau_{yx}}{\partial y} + \frac{\partial \tau_{zx}}{\partial z} \right] + g_x \quad (12.60)$$

We must modify this slightly by recognizing that some stresses result in the distortion of the fluid, a change in its shape, while some result in changes in the size of the fluid element. The mean of the normal stresses acts from all sides and can accomplish a change in volume. We define the *pressure* as

$$P \equiv -\frac{1}{3} (\tau_{xx} + \tau_{yy} + \tau_{zz}) \quad (12.61)$$

where the minus sign represents the tradition that we think about a positive pressure as one that reduces the size of an element, while our convention for normal stresses is that they were defined to be positive in tension. Given this definition of pressure, we can then decompose the stresses into those parts that result in deformation of the fluid element, called the *deviatoric stresses*, from those that can change its volume, the *pressures*:

$$\begin{aligned} \tau_{xx} &= \tau'_{xx} - P \\ \tau_{yy} &= \tau'_{yy} - P \\ \tau_{zz} &= \tau'_{zz} - P \end{aligned} \quad (12.62)$$

where the primes represent the deviatoric stresses. Rewriting each of the stress terms in the force balance equation then results in

$$\frac{\partial u}{\partial t} + u \frac{\partial u}{\partial x} + v \frac{\partial u}{\partial y} + w \frac{\partial u}{\partial z} = \frac{1}{\rho} \left[\frac{\partial \tau'_{xx}}{\partial x} + \frac{\partial \tau'_{yx}}{\partial y} + \frac{\partial \tau'_{zx}}{\partial z} \right] + g_x - \frac{1}{\rho} \frac{\partial P}{\partial x} \quad (12.63)$$

This is known as Cauchy's first law, first derived by A. L. Cauchy (1789–1857), a French mathematician (see Middleton and Wilcock, 1994, p. 307). Note that we have made no assumptions whatsoever about the nature of the materials involved. This is a very general equation reflecting conservation of momentum in an incompressible fluid. The fluid can be accelerated by either gravity or a pressure gradient.

But we are not done yet. This equation is said not to be "closed" in the sense that it is not an equation that can easily be solved for the velocity in the x -direction. The surface tractions, which come in as gradients of stresses, are not represented in terms of the flow speed, or gradients in flow speed. What is needed is a relationship between the stresses and the flow. We have some gut feeling that the flow outside of the box should push or pull or influence in some way the volume of concern. Put another way, the fluid reacts to stresses acting upon it. It does so by deforming at a given rate. This is the essence of a fluid: it responds to stresses by straining at a given rate. There is a unique relationship between stress and strain

rate in a given fluid. This relationship is called the constitutive equation, and it describes a rheology (from *rhein*, or flow). It was Newton who first described the most common of these rheologies, which he did by showing experimentally that there exists a linear relation between strain rate and stress. This may be written

$$\frac{\partial u}{\partial z} = \frac{1}{\mu} \tau_{zx} \quad (12.64)$$

This can be solved for the stress, and re-written for each component. Most generally

$$\tau_{ij} = \mu \frac{\partial u_i}{\partial x_j} \quad (12.65)$$

where i and j are indices representing x , y , or z . These expressions for stress can be plugged back into the force balance equation, yielding

$$\begin{aligned} \frac{\partial u}{\partial t} + u \frac{\partial u}{\partial x} + v \frac{\partial u}{\partial y} + w \frac{\partial u}{\partial z} = & \frac{\partial(\mu[\partial u/\partial x])}{\partial x} + \frac{\partial(\mu[\partial u/\partial y])}{\partial y} \\ & + \frac{\partial(\mu[\partial u/\partial z])}{\partial z} + g_x - \frac{1}{\rho} \frac{\partial P}{\partial x} \end{aligned} \quad (12.66)$$

If we treat first a simple system in which the viscosity is both isotropic (all 81 components representing relations between the nine components of the stress and the nine components of strain rate are equal) and does not vary in space, then we are

Box 12.5 The thermal analogy

We note that this equation is very similar to that describing the conservation of heat in a conducting medium:

$$\frac{\partial T}{\partial t} + u \frac{\partial T}{\partial x} + v \frac{\partial T}{\partial y} + w \frac{\partial T}{\partial z} = \kappa \frac{\partial^2 T}{\partial x^2} + \kappa \frac{\partial^2 T}{\partial y^2} + \kappa \frac{\partial^2 T}{\partial z^2} + S \quad (12.70)$$

The gravity and pressure gradient terms serve as sources of momentum, just as radiogenic elements serve as the sources of heat, S , in the general heat equation. The gradients in stresses serve the same purpose as the gradients in heat flow, and are reflected in curvature of velocity on the one hand, and of temperature on the other hand. The analogy is made even tighter by recognizing that the position of the kinematic viscosity in the equation is analogous to the position of the thermal diffusivity. In fact, they have the same units.

Let us classify this Navier–Stokes equation. It is a partial differential equation for u -velocity (or speed), in that it contains derivatives of both time and all three spatial variables. It is second order, as the highest order of derivative is the second-order terms on the right-hand side. And it is nonlinear, in that the advective terms on the left-hand side contain products of the variable u and its derivatives. It is this latter quality that makes this equation particularly difficult to solve for the most general cases.

justified in pulling viscosity out of the derivatives, yielding three terms dependent upon the curvature of the velocity profile:

$$\frac{\mu}{\rho} \frac{\partial^2 u}{\partial x^2} + \frac{\mu}{\rho} \frac{\partial^2 u}{\partial y^2} + \frac{\mu}{\rho} \frac{\partial^2 u}{\partial z^2} \quad (12.67)$$

The collection of two constants in front of each term arises so commonly in fluid mechanics problems that they have been given their own name, the kinematic viscosity:

$$\nu = \mu/\rho \quad (12.68)$$

which has dimensions of L^2/T . Our final equation for the conservation of momentum in the x -direction is then

$$\frac{\partial u}{\partial t} + u \frac{\partial u}{\partial x} + v \frac{\partial u}{\partial y} + w \frac{\partial u}{\partial z} = \nu \frac{\partial^2 u}{\partial x^2} + \nu \frac{\partial^2 u}{\partial y^2} + \nu \frac{\partial^2 u}{\partial z^2} + g_x - \frac{1}{\rho} \frac{\partial P}{\partial x} \quad (12.69)$$

This is the x -component of the *Navier–Stokes equation*. The French engineer Claude Navier (1785–1836) and the English mathematician George Stokes (1819–1903) derived this equation in the early nineteenth century, a step beyond Cauchy's first law taken by representing the deviatoric fluid stresses with a viscous rheological law. There are two other equations for the other two components of momentum, y and z , which we will leave to the reader to write.

The assumptions that we have used to arrive at this form of the equation are:

- the material is incompressible;
- the material behaves as a linear viscous fluid;
- the viscosity does not vary spatially.

Non-dimensionalization of the Navier–Stokes equation

It would be immensely helpful to the solution of this equation if we could simplify it by being able to ignore one or another term. One approach is to determine formally how large each of the terms is in a particular problem. Those that are large relative to others are retained, while those that are small are ignored. This is accomplished by scaling the equation, and converting it to a dimensionless form. Each of the variables can be scaled by a characteristic scale in the particular problem; this is an exercise in normalization. For example, the length scales in a grain settling problem will be the diameter (or the radius) of the particle (which we choose is in part dictated by tradition!). The velocity scale in open channel flow might be taken to be either the surface velocity or the mean velocity. This can be achieved by defining

$$T' = t/T, x' = x/L, y' = y/L, z' = z/L, \quad (12.71)$$

$$u' = u/U, v' = v/U, w' = w/U$$

where T , L , and U are the characteristic scales chosen for time, length, and velocity, respectively, and the primes indicate new, non-dimensionalized variables. These definitions can be used in rewriting the original equation to become

$$\begin{aligned} & \left[\frac{U}{T} \right] \frac{\partial u'}{\partial t'} + \left[\frac{U^2}{L} \right] u' \frac{\partial u'}{\partial x'} + \left[\frac{U^2}{L} \right] v' \frac{\partial u'}{\partial y'} + \left[\frac{U^2}{L} \right] w' \frac{\partial u'}{\partial z'} \\ & = \left[\frac{U}{\nu L^2} \right] \frac{\partial^2 u'}{\partial x'^2} + \left[\frac{U}{\nu L^2} \right] \frac{\partial^2 u'}{\partial y'^2} + \left[\frac{U}{\nu L^2} \right] \frac{\partial^2 u'}{\partial z'^2} + g_x - \left[\frac{1}{\rho} \frac{P_o}{L} \right] \frac{\partial P'}{\partial x'} \end{aligned} \quad (12.72)$$

Here we have collected all the scales in the problem into the square brackets. The remaining variables and gradients are not only dimensionless, but should have values that are of the order of 1 to a few, if we have done our scaling correctly (and this is the art of the exercise). The magnitudes are then all carried by the scales in the brackets. It is by comparing the magnitudes of these collections of constants in brackets that one can assess the relative importance of one or another term in the equation. There is one more step, which makes this comparison even easier. If we divide all of the terms by the scales in front of, say, the inertial or advective acceleration terms, the resulting equation will be rendered dimensionless. Even more importantly, the dimensionless numbers in front of each term will reflect the importance of that term relative to the inertial terms. Let us do this:

$$\left[\frac{L}{UT} \right] \frac{\partial u'}{\partial t'} + [1] u' \frac{\partial u'}{\partial x'} + [1] v' \frac{\partial u'}{\partial y'} + [1] w' \frac{\partial u'}{\partial z'} \quad (12.73)$$

$$= \left[\frac{\nu}{UL} \right] \frac{\partial^2 u'}{\partial x'^2} + \left[\frac{\nu}{UL} \right] \frac{\partial^2 u'}{\partial y'^2} + \left[\frac{\nu}{UL} \right] \frac{\partial^2 u'}{\partial z'^2} + \frac{g_x L}{U} - \left[\frac{P_o}{\rho U^2} \right] \frac{\partial P'}{\partial x'}$$

Assure yourself that each of the terms in the brackets is dimensionless. These dimensionless numbers, or slight rearrangements of them (their inverse, or one half of them) are the important dimensionless numbers of fluid mechanics. They are as follows:

$$\text{Re, Reynolds number} = \frac{UL}{\nu}$$

$$\text{Fr, Froude number} = \frac{U}{\sqrt{g_x L}} \text{ (pronounced Froud)}$$

$$\text{Eu, Euler number} = \frac{P_o}{\frac{1}{2} \rho U^2}$$

$$\text{St, Strouhal number} = \frac{UT}{L}$$

Given these dimensionless numbers, all named for famous mathematicians and fluid mechanicians, we can now re-write the last equation to yield

$$\left[\frac{1}{St} \right] \frac{\partial u'}{\partial t} + [1]u' \frac{\partial u'}{\partial x} + [1]v' \frac{\partial u'}{\partial y'} + [1]w' \frac{\partial u'}{\partial z'} \\ = \left[\frac{1}{Re} \right] \frac{\partial^2 u'}{\partial x'^2} + \left[\frac{1}{Re} \right] \frac{\partial^2 u'}{\partial y'^2} + \left[\frac{1}{Re} \right] \frac{\partial^2 u'}{\partial z'^2} + \frac{1}{Fr^2} - [2Eu] \frac{\partial P'}{\partial x'} \quad (12.74)$$

It should now be clear that the utility of these numbers is that they allow us to determine rapidly the importance of each term relative to the inertial term. Most important for our purposes now is the Reynolds number. Note that if Re is small, then the magnitude of the viscous terms becomes large compared to the inertial terms. The latter can then safely be ignored. As these inertial terms are the nonlinear ones, this is tremendously useful. The Reynolds number is small if the product of the length and velocity scales is small compared to the kinematic viscosity. This number was named for Osborne Reynolds

(1842–1912), a civil and mechanical engineering professor at Owens College, Manchester, working in the late nineteenth century on the onset of turbulence in flow through tubes, although George Stokes (1819–1903) had pointed out the importance of this collection of constants in controlling the flow field for particular geometries 40 years earlier (e.g., what we now call Stokes law for the drag force on a sphere; see Batchelor, 1970, p. 214). Reynolds published a pair of papers that have become pillars in turbulence research (Jackson and Launder, 2007). In the first he reported his experiments on the “tendency of water to eddy” and the control of this tendency by a ratio of scales that now carries his name (Reynolds, 1883), and a theoretical approach to averaging of the Navier–Stokes equations (to yield what are now known as the Reynolds equations) as a means of exploring the switching of flows into and out of turbulence (Reynolds, 1895).

Problems

1. Estimate the time it takes for a water molecule to travel from the source of the Amazon to the ocean.
2. *Flow competence.* Assess the maximum diameter grain capable of being entrained by a flow 2 m deep, travelling down a channel with a slope of 0.002. The particles are granitic and have a density of 2700 kg/m³. Use the simple expression presented in the text, employing the Shield’s parameter of $\theta = 0.06$. Give the diameter in mm.
3. A commonly used bedload transport formula in fluvial settings is the Meyer–Peter–Muller formula. A simple version of this is $Q = A(\tau_b - \tau_c)^{3/2}$, where $A = 0.04$ (the units of A work out such that Q is in kg/(m s), and shear stresses are in N/m²). Using this formula, and a coarse sand of diameter $D = 5$ mm in the channel, and flow conditions described in question 2, what do you expect for the discharge of sand in this channel? Give your answer in kg/s.
4. *Mississippi River velocity structure and sediment transport.* You are given a set of measurements of the flow velocity within a profile of the Mississippi River, at this place and time flowing with a flow depth of 8.5 m. The measurements are as follows:

z (m above bed)	U (m/s)
7.7	1.25
5.2	1.20
3.2	1.05
1.8	1.00
0.9	0.90
0.6	0.80

 - (a) Recalling the *law of the wall*, what is your best estimate of the shear velocity, u_* ? What is the roughness length of the flow, z_o ? (*Hint*: recall von Karman’s constant, $k = 0.4$.) Plot your results in both linear–linear and log–linear fashion (linear in U as the x -axis and log of z on the y -axis), showing both the data and

your predicted velocity structure, using your best estimates for u_* and z_0 .

- (b) Given this, what is the slope of the river in this reach? (Note that this is actually a very difficult measurement to make in these cases.) You will have to use the definition of the shear velocity for this calculation:

$$u_* = \sqrt{gHS}$$

- (c) Would coarse quartz silt of diameter 0.125 mm be in suspension here? (*Hint*: the criterion for suspension is that the Rouse number $p < 2.5$, see Chapter 14.)

5. *Fluid discharge.* Consider a steep-walled river channel with a width of 50 m, a bankfull depth of 3 m (to the levee tops), and a slope of 0.5 m/km (i.e., note that this is the tangent of the slope, which for small angles is equivalent to the slope, in radians: 0.0005). The bed of the river is made of coarse sand, organized into ripples that result in an effective roughness length (z_0) of 3 mm. The river at the moment is flooding at a stage of 0.5 m above bankfull. Recall that the shear velocity u_* is defined as $u_* = \sqrt{\tau_b/\rho}$, or $u_* = \sqrt{gHS}$. Calculate the water discharge in the channel, in m^3/s :

(a) at bankfull;

(b) at 0.5 m above bankfull (i.e., at present).


(Note that in both cases you may ignore the effects of the banks, which will be small relative to the bottom in imposing friction on the flow.) In the latter calculation, ignore the contribution from that flow that escapes over the floodplain.

6. You now obtain a water sample of the same river from a specific depth, 10 cm above the bed, and have its grain-size distribution analyzed. There are three primary grain diameters involved (all quartz; assume that they are all essentially spherical), and their sizes and concentrations at this level in the flow are as follows:

D1	0.25 mm	45 mg/L
D2	0.17 mm	30 mg/L
D3	0.01 mm	20 mg/L

- (a) What is the Rouse number, p , of each of the grain sizes when the flow is 0.5 m above bankfull? (See Chapter 14.)
- (b) Plot the expected concentration profiles of these grains as a function of height above the bed, using height (z) as the vertical axis on your plot. First plot the profiles on a linear-linear plot, then on a log-log plot.
- (c) What is the *mean* concentration of sediment (of each grain size) in that part of the flow that goes overbank?
7. For a given discharge of a river, calculate and plot the dependence of the river stage on the roughness of the bed of the river. (This is relevant to management plans for how to modify a river to maximize the water it can pass below a given stage.)
8. Estimate the mean residence time of a sand grain on a floodplain. Assume that the sand grain was deposited in a scrollbar deposit as the river meandered within the floodplain. The floodplain is neither aggrading nor eroding. The floodplain width is 5 km, the channel width is 80 m, and aerial photos indicate that it is migrating laterally at a mean rate of 10 cm/year.
9. *Thought question.* Given your answer to this last question, contemplate how this would be reflected in the concentration of ^{10}Be in the sand contributed to the river from bank erosion.
10. *Thought question.* Discuss how rivers might differ if the fluid being transported were of a different density or viscosity, or both. (And lest you think this silly, we are learning about a landscape on Titan that appears to have been in part sculpted by liquid methane.)

Further reading



Dunne, T. and L. B. Leopold, 1978, *Water in Environmental Planning*, San Francisco, CA: W.H. Freeman Co., 818 pp.

This text sets the bar for an environmental planning book, bringing the science of water in the landscape to the planner.

Henderson, F. M., 1966, *Open Channel Flow*, New York: Macmillan, 522 pp.

This is a well-organized textbook that many turn to for clear discussion of river mechanics problems.

Knighton, D., 1998, *Fluvial Forms and Processes: A New Perspective*, 2nd edition, Oxford: Arnold, 400 pp.

This text provides a more up-to-date analysis of river mechanics and its landforms than that given in Leopold,

Wolman and Miller. This updated version of the text leans heavily on recently collected data, and draws on river studies from around the world.

Leopold, L. B., 1994, *A View of the River*, Cambridge, MA: Harvard University Press, 290 pp.

This very readable book provides a window into what Luna Leopold thought about rivers, over the many decades in which he was involved in their study and in their protection.

Leopold, L. B., M. G. Wolman, and J. P. Miller, 1964, *Fluvial Processes in Geomorphology*, San Francisco, CA: W. H. Freeman, 522 pp.

This is a classic, written by those who brought the mechanics of rivers into the geomorphic realm.